NASA-CR-167948
19820023633

NASA CR-167948

NASA

ION BEAM MICROTEXTURING AND ENHANCED SURFACE DIFFUSION

PREPARED FOR

LEWIS RESEARCH CENTER

NATIONAL AERONAUTICS AND SPACE ADMINISTRATION

GRANT NAG 3-43

Final Report

February 1982

Raymond S. Robinson

Department of Physics
Colorado State University
Fort Collins, Colorado 80523

1 Report No	2 Government Accession No	3 Recipient's Catalog No
CR-167948		

4 Title and Subtitle	5 Report Date
Ion Beam Microtexturing and Enhanced Surface Diffusion (U)	February 1982
	6 Performing Organization Code

7 Author(s)	8 Performing Organization Report No
Raymond S. Robinson	
	10 Work Unit No

9 Performing Organization Name and Address	11 Contract or Grant No
Physics Department Colorado State University Fort Collins, CO 80523	NAG 3-43
	13 Type of Report and Period Covered
12 Sponsoring Agency Name and Address	Contract Report
National Aeronautics and Space Administration Washington, DC 20546	14 Sponsoring Agency Code

15 Supplementary Notes

Grant Manager Maris A. Mantenieks
NASA Lewis Research Center
Cleveland, OH 44135

16 Abstract

Work under this Grant has been primarily in the area of ion beam interactions with solid surfaces with particular emphasis on microtexturing induced by the deliberate deposition of controllable amounts of an impurity material onto a solid surface while simultaneously sputtering the surface with an ion beam. Experimental study of the optical properties of microtextured surfaces is described. Measurements of both absorptance as a function of wavelength and emissivity are presented. The behavior of a quasi-liquid coating that develops on the surface of a cone is also described. This coating develops during sputtering and simultaneous seeding and its properties are important in understanding the processes of cone formation, development, and removal. Ion beam enhanced surface diffusion is discussed in which the impacting ions are responsible for a large increase in adatom mobility on the surface above the mobility due to equilibrium thermal effects. A computer code is described that models the sputtering and ion reflection processes involved in microtexture formation.

17 Key Words (Suggested by Author(s))		18 Distribution Statement
Texturing	Ion Beam	Unclassified, unlimited
Sputtering	Ion Source	
Microtexturing	Seeding	
Diffusion	Surfaces	

19 Security Classif (of this report)	20 Security Classif (of this page)	21 No of Pages	22 Price*

* For sale by the National Technical Information Service, Springfield, Virginia 22161

TABLE OF CONTENTS

LIST OF FIGURES AND TABLES

I. INTRODUCTION

Work under this Grant has been primarily the study of ion beam interactions with solid surfaces with particular emphasis on micro-texturing induced by the deliberate deposition of controllable amounts of an impurity material onto a solid surface while simultaneously sputtering the surface with an ion beam.[1-3]

Ion beam microtexturing is not only a useful means of obtaining information about some of the basic processes on surfaces that are related to ion beam texturing but has a number of areas of practical application as well. Textured surfaces obtained by using other methods have been used as radiant energy absorbers.[4] Texturing has been used to prepare surfaces for biomedical applications involving intimate contact with tissue.[5-8] Textures have also been applied to heat transfer surfaces[9] and electron emitters.[10,11]

The techniques for producing textured surfaces include CVD,[4,12-14] chemical etching[15] and sputtering.[11,16-18] The first two techniques are limited in application due to material constraints. At present, work on CVD techniques has centered on W and Rh dendrites on sapphire, W, and stainless steel. This method is generally limited to substrates that can be "wetted" by W. The chemical etching process has only been demonstrated in Si. By taking advantage of the crystal structure, small pyramids can be etched into the surface with suitable etchants.

The sputter-texturing technique has several advantages over these other techniques. The most prominent of these is the ability to use a wide range of substrates. At least 26 different materials have been demonstrated to texture, and most vacuum compatible materials would be expected to texture under the proper conditions. Another advantage of

the sputter texturing technique is relative purity. The impurity seeding levels are typically 0.2 → 2% of the bulk concentration. This means that, for example, a copper textured surface is mostly copper and has for the most part thermal conduction and expansion coefficients characteristic of copper. A third advantage is the lack of a separate film layer on the surface. The cones are actually etched into the surface; they cannot later peel off as a deposited layer might. Finally, the texturing can be formed over a range of temperatures.

In this report various properties of sputter-textured surfaces are presented. The absorptance and emissivity of various textured surfaces (see Table 1) were measured.

Detailed observations have been made of the quasi-liquid behavior of the coatings that develop on sputter cones. The observed properties of these coatings depend on the presence of both the deposited impurity and the continual bombardment by the primary ion beam.

Impact enhanced surface diffusion during impurity induced sputter cone formation was studied as a function of the incoming ion beam current density.

Work has also progressed on a computer code that models the development of a sputtered surface, taking into account the variation in both sputter yield and ion reflection with angle of ion beam incidence. This model is capable of presenting a time development of various prescribed initial surface topographies in two dimensions.

Earlier reported work under this Grant[19,20,21] focused primarily on two experimental studies. The first experimental study involved the detailed time development of impurity seeded sputter cones in which the formation and long-term development of individual cones was observed.

An overlying coating was discovered on cones that is apparently a combination of seed and substrate materials that exhibits a depressed sputter yield relative to the bulk substrate material. Another subject of considerable experimental study was the measurement of surface diffusion activation energies as they relate to impurity-induced cone density. Activation energies were interpreted according to a thermodynamic model of surface texturing developed earlier.[22,23] Measurements were made on 29 different combinations of impurity seed and solid substrate materials.

Additional observations were made of the apparent crystal structure of the bases of cones in contact with a solid substrate. Both hexagonal and rectangular structures were observed, sometimes on the same sample but on different crystal grains. A correlation was also found between the critical temperature for the onset of texturing on a variety of materials and the bulk sputtering rate of the substrate.

Experimental work under this Grant including operation of the scanning electron microscope has been carried out primarily by Stephen M. Rossnagel, a physics graduate student at Colorado State University. Mr. Rossnagel also carried out the digital simulations of ion beam sputtering.

II. APPARATUS AND PROCEDURE

The apparatus and procedure used to carry out the experiments were essentially the same as previously used[19] and are included here for completeness.

Textured surfaces can be generated by simultaneously sputtering a surface at high energy while seeding it with impurity atoms at low energy. A broad-beam ion source is used that produces a low energy (50-1500 eV) high intensity (0-2.7 mA/cm^2) beam which was neutralized using a thermionic filament immersed in the beam. This system allows a high degree of beam control and a moderately low background pressure ($\sim 10^{-5}$ Torr) in the sputtering region. High vacuum was obtained using a closed-cycle cryopump for an oil-free environment ($\sim 10^{-8}$ Torr no load pressure). Argon was used as the source gas at a typical ion energy of 500 eV and at a current density of 1.0 mA/cm^2. The beam diameter was 5 cm at the ion optics and no beam defining apertures were used. There have been other reported studies which find sputtered aperture material to be an additional impurity at the surface, itself capable of initiating cone formation.[24] The samples were mounted normal to the beam at a distance of 25 cm from the source. They were mounted on a temperature controlled copper holder with a thermocouple mounted directly behind the sample. The sample and the holder were both polished and clamped tightly together. The holder was constructed in such a way that the sides of the holder sloped away from the sample, reducing possible contamination effects seen by others.[25]

The impurity or seed source consists of a target of the chosen seed material placed in the edge of the ion beam between the ion source and the sample. This target was placed at an angle to the beam such that

some of the atoms sputtered from its surface impinged on the sample surface (Fig. 1). The magnitude of the impurity seed flux can be controlled by the amount of the target exposed to the beam and the positioning of the impurity target in the beam. Because the impurity source was large compared to the sample (20 cm^2 vs. 1 cm^2), and the target and substrate were typically separated by a few centimeters, the impurity flux to the sample can be considered uniform over the sample area. Strong gradients in seed flux have been treated earlier.[2] The magnitude of this flux depends on the materials tested and has been experimentally measured to be from 0.2 to 3 percent of the ion beam flux.

The samples to be textured were either foils or thin sheets and were cut into 1 cm^2 squares. All of the samples for each metal substrate used were cut from a single piece, thereby assuring the thickness and purity to be the same. All samples, as well as impurity materials, were at least 99.95% pure and were polycrystalline. No attempts were made to determine the crystal structure or to use single crystal samples. The thicker samples were polished mechanically to an approximate mirror finish, and all samples were then ultrasonically cleaned in Alconox, acetone, then ethanol. The samples were then immediately mounted on the sample holder, evacuated to at least 10^{-7} Torr, and heated to the desired temperature in vacuum. The subsequent exposure to the ion beam and seed flux varied, depending on the type of experiment. For studies of impact enhanced diffusion, the beam current density was varied from 0.1 to 2.7 mA/cm^2.

Additional procedures include the use of a Beckman spectrophotometer operating in reflectometer mode to measure reflectance from textured

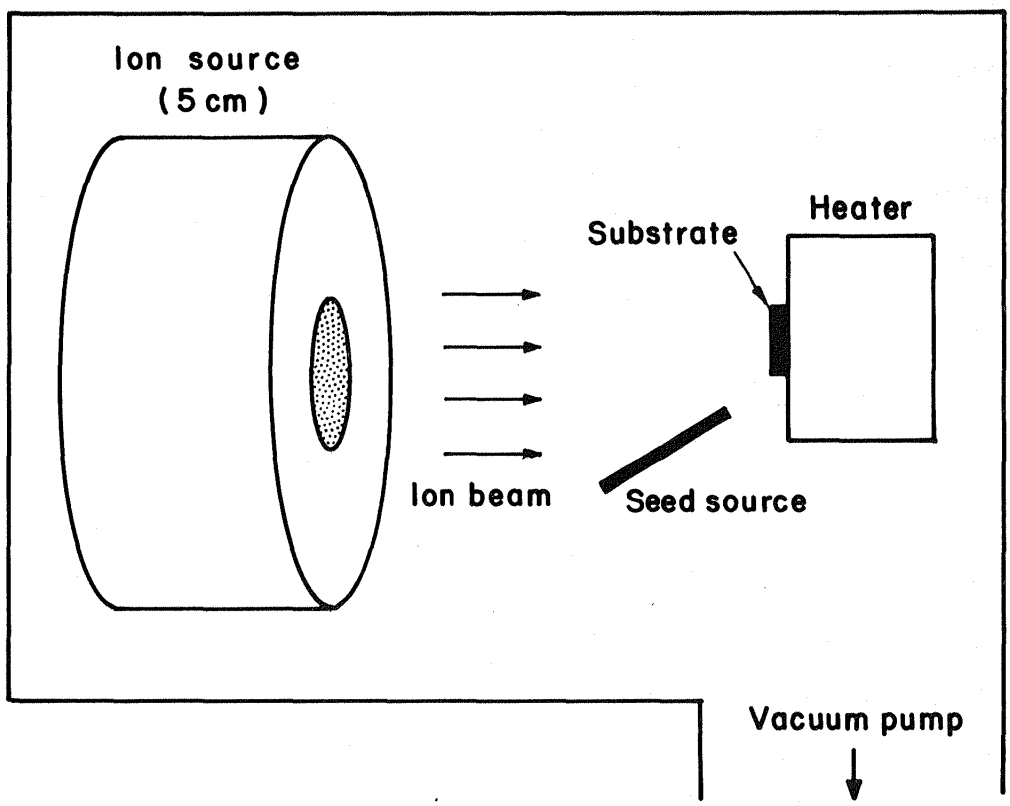

Fig. 1. Schematic of experimental apparatus for microtexturing. The seed source is movable.

samples as a function of wavelength. The absorptance was then calculated by subtracting the reflectance from unity. When average values are quoted, the averages were taken over the measured wavelength interval. A thermocouple arrangement was used to monitor the vacuum cooling of samples to determine the emissivity. The emissivity can be measured by the rate of cooling in vacuum. Textured samples were suspended by fine thermocouple wires in a vacuum oven. After heating at 700°C, the samples were removed to a cold part of the vacuum chamber to cool. From the cooling rate, the emissivity was deduced.

III. OPTICAL PROPERTIES OF TEXTURED SURFACES

Textured surfaces have been found suitable as radiant energy absorbers. The optical properties of these textured surfaces obtained by various methods have been described by other investigators. The present study was directed toward measuring the absorptance and emissivity of various ion-beam textured surfaces. Six different substrate materials were textured to produce high absorption. Examples of such textured surfaces are shown in Fig. 2. The absorptance was measured with a Beckman 2-D spectrophotometer over the range 0.35-2.25 μm. The emissivity was measured by the rate of cooling in a vacuum. The results of the measurements of optical properties of ion beam textured surfaces are shown in Table 1. Absorptance values were found to vary between 0.95 and 0.98 for all textured surfaces except Al substrates. Aluminum textured with Fe and Mo yielded absorptances of only 0.90. A typical example of absorptance measured as a function of wavelength over a 0.35-2.25 μm range is shown in Fig. 3. The measured values of absorptance are in good agreement with those obtained by other workers.[4,26] It is probable that the absorption is a result of multiple reflections in the closely-spaced texture. If the spacing of the texture is on the scale of the incident light the absorptance can be quite high.

In one case, the Si substrate, the absorptance was measured also as a function of incidence angle of light from 0 to 60°. No change in absorptance was observed.

Emissivity is also an important parameter for solar absorbers. Low emissivity in a solar absorber can prevent the loss of a great deal of the incident energy when the absorber is hot. Ion beam textured

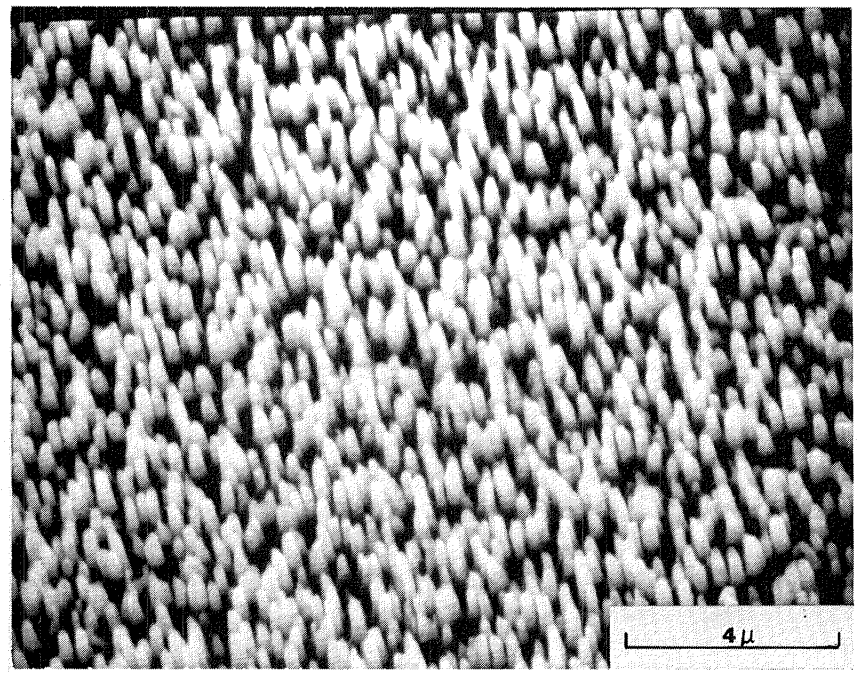

(a) Dense Cu induced structure on Si. Ar^+, 500 eV, 1×10^{19} ions/cm^2.

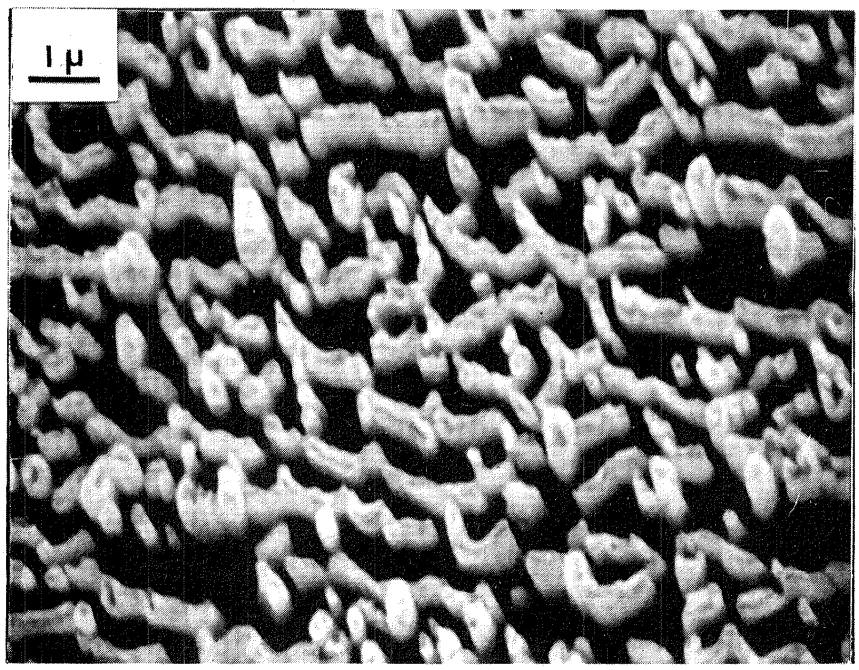

(b) Wavelike formations, W induced structures on Cu. Ar^+, 1000 eV, 2×10^{18} ions/cm^2.

Fig. 2. Examples of microtextured surface topography exhibiting high optical absorption.

Table 1. Optical Measurements for Ion Beam Microtextured Surfaces.

Substrate	Impurity	Absorptance (0.35-2.25 μm)	Emissivity
Cu	W	0.96	0.2-0.3
	Mo	0.96	0.2-0.3
	Fe	0.96	-
	S.S.	0.96	-
Ni	W	0.97	0.2-0.3
Si (0-60°)	Cu	0.98	-
	Mo	0.96	-
	Ta	0.95	-
	Fe	0.95	-
Brass	Fe	0.95	-
Al	Fe	0.90	-
	Mo	0.90	-
Graphite	Fe	0.97	-

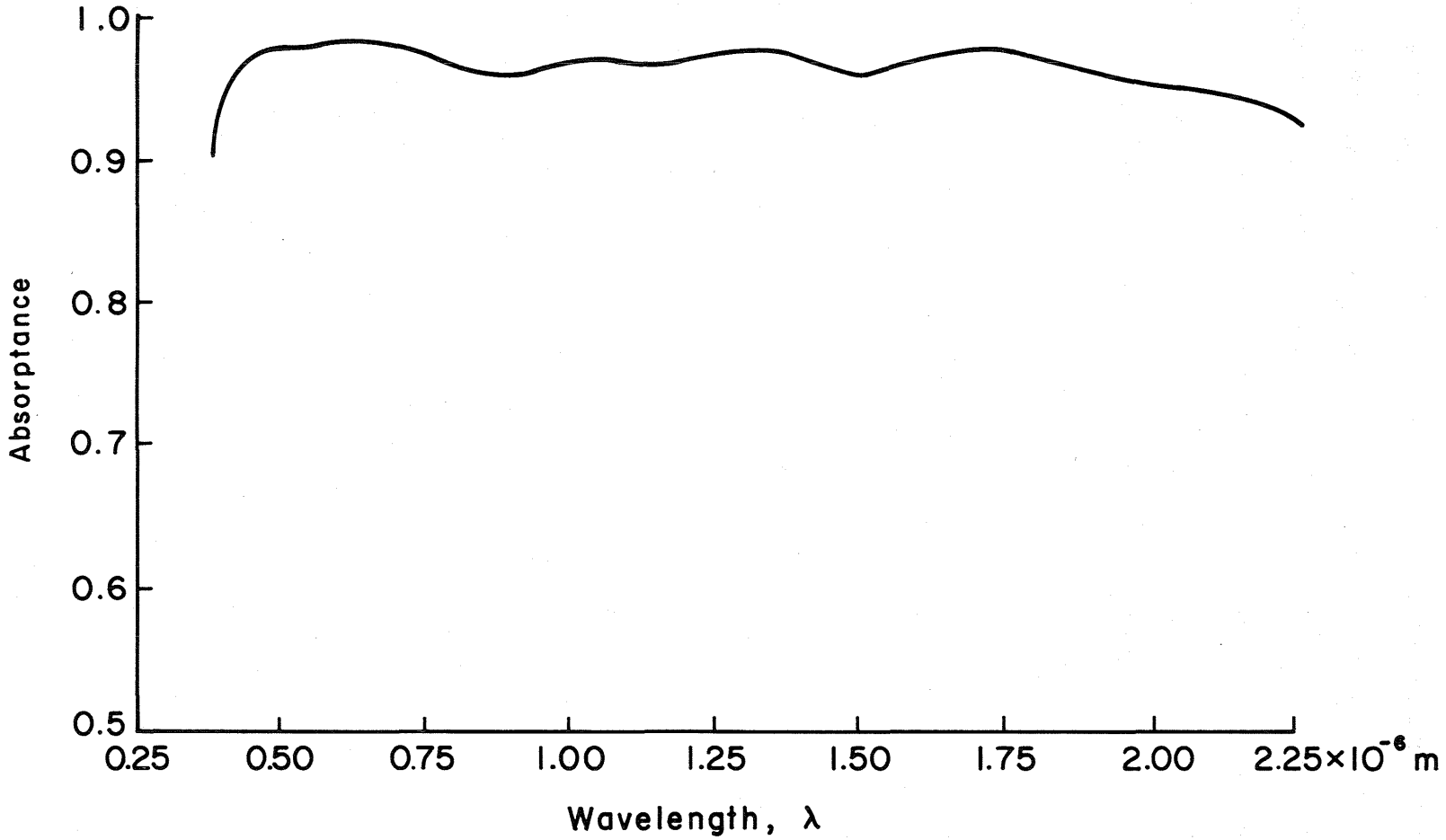

Fig. 3. Absorptance as a function of wavelength of incident light for W induced structures on Ni.

surfaces of suitable dimensions also offer favorable emissivities as well as high absorptance. The measured emissivities of Cu and Ni substrates were found to be 0.2 - 0.3 (Table 1). The measured emissivities are in good agreement with those obtained for metallic dendritic absorbers measured by similar techniques.[4] The values are, however, lower than those measured by Hudson et. al.[26] on ion beam textured surfaces.

IV. QUASI-LIQUID BEHAVIOR OF CONE COATINGS

Upon careful observation of cone features, particularly during the cone formation and growth, a coating has been observed on the surface of the cones.[20] This coating is related to cone stability as well as growth.[20] The coatings are generally 100-2000 Å thick, and have been shown via AES and EDAX to have low levels of the added impurity ($\lesssim$2% atomic) with no apparent concentration gradient across the cone surface. In particular, no pure clusters were found at the top of the cones. The areas between the cones have much lower impurity levels (<0.2% atomic). The absence of the pure cluster complicates the simple model developed earlier.[22] The coatings are clearly observed with several seed-substrate combinations but are not detectable with scanning electron microscopy when some other material combinations are used. However, when observed, the coating is clearly directly related to the development and subsequent failure of the cone. The type of impurity has some effect on the extent of the observed liquid-like properties. Some systems, such as C on Cu and Al on Cu have a much more evident coating, and the liquid-like features are more prominent. Some evidence of the coating and the liquid-like features were observed on other substrates such as Al, Pb, Au, and Ni during the course of our experiments.

A feature often seen in the early development of the impurity-induced cone structures is a droplet structure, a ball on a thin pedestal extending from the surface (Fig. 4). These structures can be quite small, with balls of 2000 Å diameter and pedestals down to 100 Å in diameter at their thinnest point. These droplet structures are also seen later in the cone development (e.g., Fig. 5) protruding from the

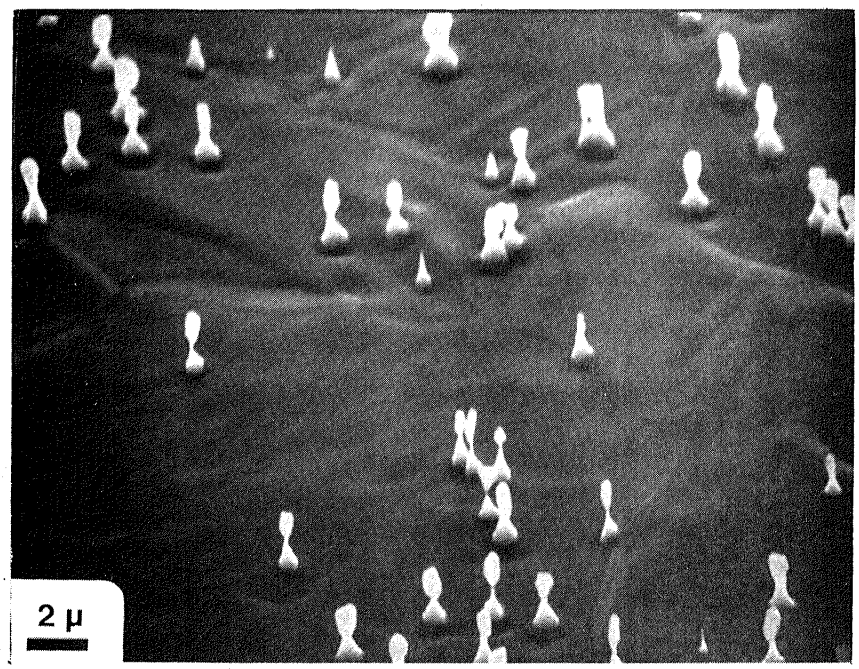

(a) 420°C, 1×10^{19} ions/cm^2, Ar^+ 1000 eV, 2 mA/cm^2.

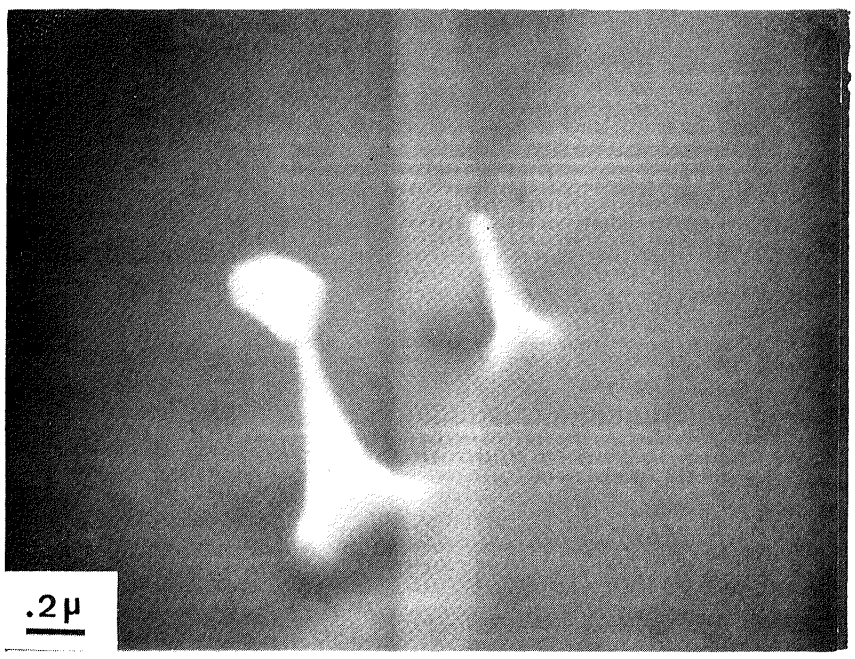

(b) 420°C, 9×10^{18} ions/cm^2, Ar^+ 1250 eV, 1 mA/cm^2.

Fig. 4. Carbon induced cones on copper.

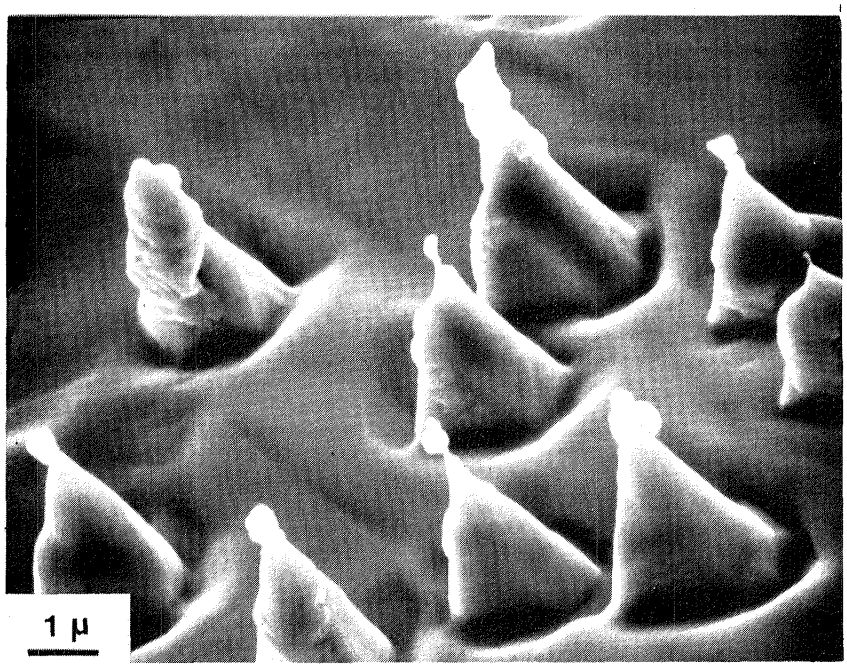

(a) 300°C, 7×10^{18} ions/cm^2.

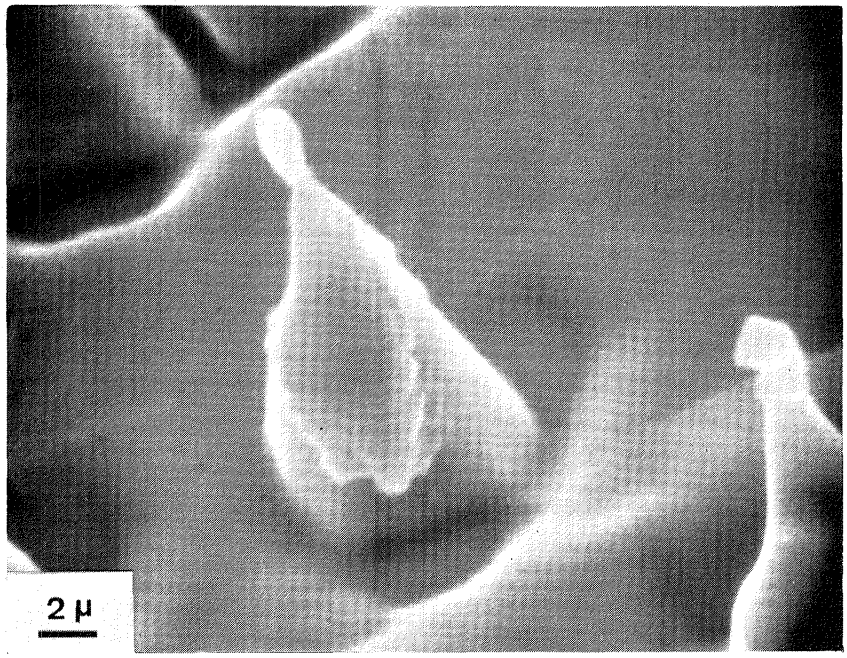

(b) 300°C, 1×10^{19} ions/cm^2.

Fig. 5. Carbon induced cones on copper exhibiting quasi-liquid coating behavior.

tops of much larger cone structures. At the bases of the droplet structures, what appear to be wetting angle effects are observed as in Fig. 4b or 5b.

The coating often has the appearance of a "viscous liquid,"[20] even at temperatures as low as 300°C on Cu even though the actual melting point is 1083°C. This "quasi-liquid" behavior is evidenced by the "dripping" and "rippling" in the coating on the cone sides (Fig. 5). Another apparent surface tension effect is in the sequence of events during cone failure.[20] The coating on the cone develops an opening at the cone apex. This opening forms not as the coating is simply worn away, but the coating apparently tends to pull away from the tip, forming a distinct edge in the coating. Another feature that implies liquid-like behavior is the production of wave-like or winding structures often seen while sputtering in the presence of impurities (Fig. 2b). These structures are produced at certain combinations of temperature and seeding density. At lower temperatures, or lower seeding fluxes, the same system that will develop wave-like structures (e.g., Ta on Cu) will produce separated cones. The production of these structures appears to require flow or agglomeration of the coating material between adjoining cones although the dynamics of such a process have not been observed directly. This is demonstrated to some degree by certain structures having an intermediate appearance (Fig. 6). The effect can be seen to some extent on single cones late in their development. Once the coating has opened, exposing the underlying tip of the bulk material, the coating may form a circular ring of second-generation cones around the top.[20] These can partially flow together to form the "hollow" cones first described by Wehner.[3]

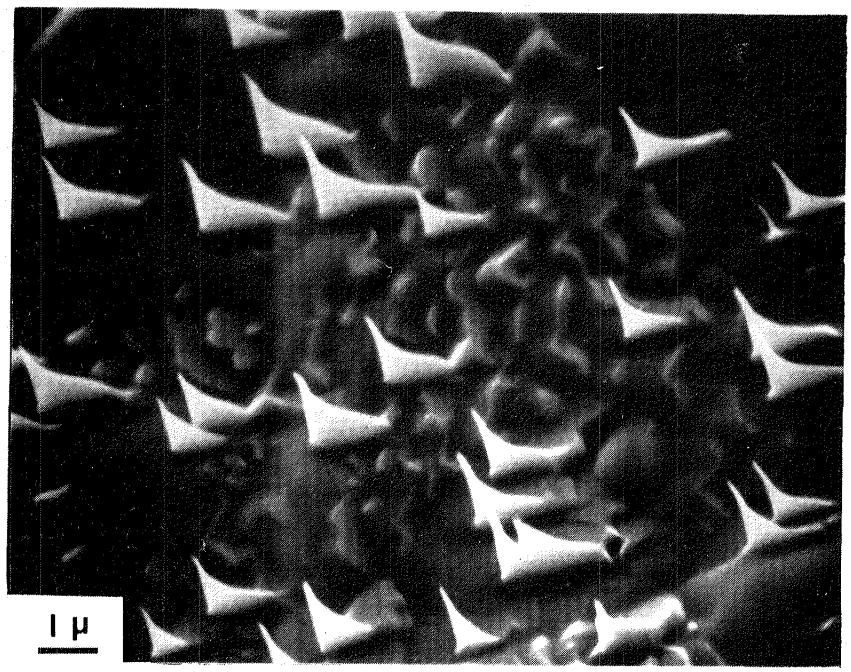

Fig. 6. Tantalum induced structures on copper, 500°C, 1×10^{19} ions/cm^2.

The bulk temperatures reached in these observations are well below the bulk melting points or the individual system eutectics. Typical values are 250-500°C for various impurities on Cu and 100-400°C on Au. The ion beam produces a power flux in the range 0.1 to 2 watts/cm^2 which causes moderate temperature increases in bulk temperatures of 10-15°C at 300°C. At higher temperatures (500°C) this flow or quasi-liquid effect is reduced. Because of the moderate temperatures, melting does not appear to be involved. In the absence of conventional melting, "quasi-liquid" has been used to describe the apparent mobility and flowing observed.

The bulk temperature, although not high enough to produce melting, does have an effect on the resultant cone size and shape. On Cu at low temperatures (250-300°C) the structures tend to be broad-based pyramids. At intermediate temperatures (350-450°C), the structures are narrower at the base, with occasional quasi-spherical structures on the tips. At high temperatures, ($\gtrsim$450°C), the resultant form is narrow based with a narrow neck and large droplet structures on the tips (Fig. 5).

One additional observation that may be related to these liquid-like features is the occurrance of cone bending. This can range from minor deflection at the tip, to dramatic bending of the upper two-thirds of the cone (Fig. 7). The bending can be induced by placing a hot filament near the surface of the sample for a few seconds while the ion beam is on. Bending does not occur in the absence of the ion beam. The estimated power flux at the cone due to this radiant heating is $\sim$2-5 watts/cm^2. The cones generally bend away from the heat source. It should be noted that the experimental conditions for texturing were not identical in Figs. 7(a) and 7(b).

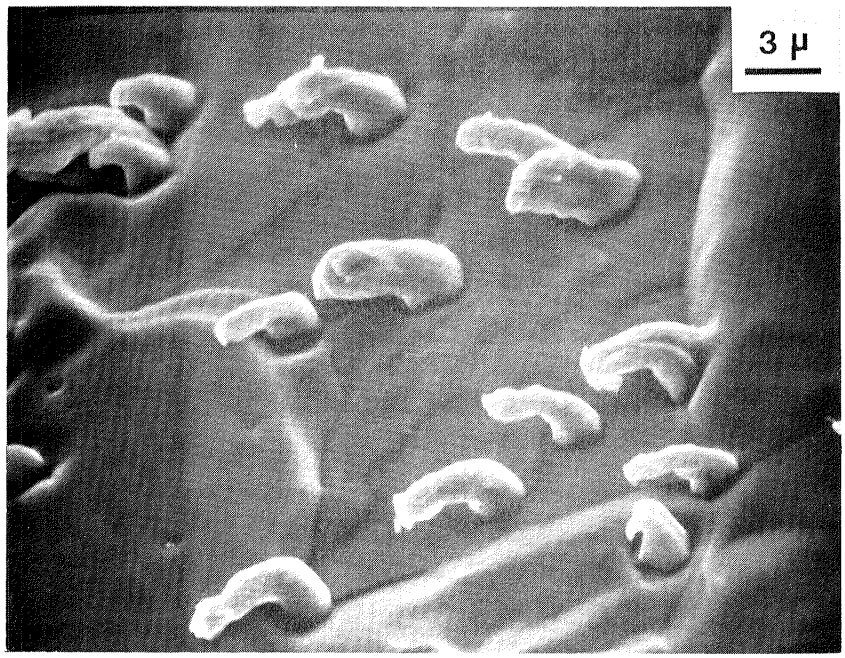

(a) Carbon induced cones on copper heated from the right.

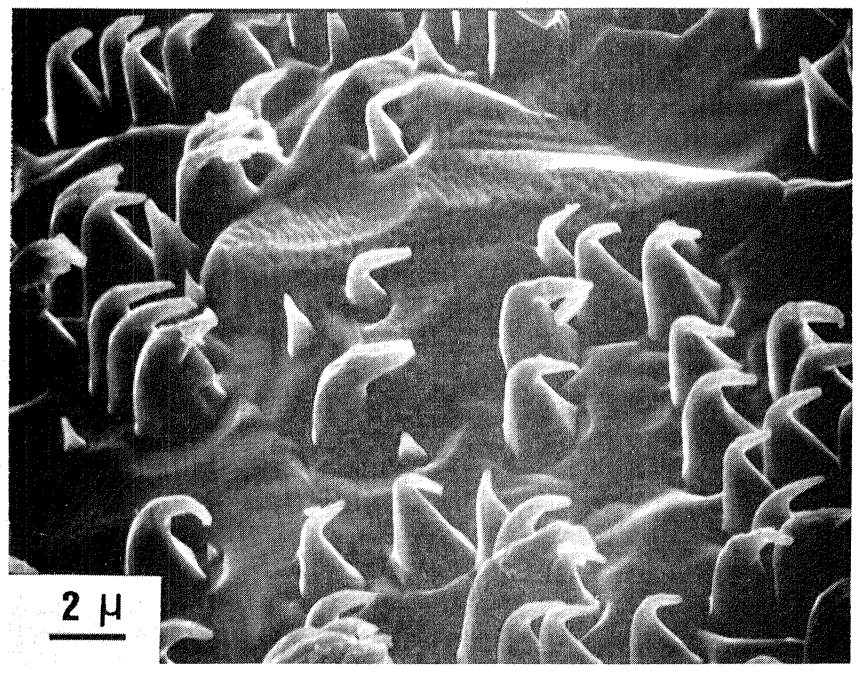

(b) Carbon induced cones on copper heated from the left.

Fig. 7. Cones bent by heating from one side during ion bombardment.

Each of the effects described; the dripping and rippling, the droplets, the wetting angle and surface tension effects, the winding structures, the cone failure mode, and the cone bending, seem characteristic of some sort of macroscopic motion in the coating on the cone surface. Many of the resulting structures cannot be explained by means of simple sputtering, reflection and redeposition. The winding or wavelike structures and the droplets seem specifically indicative of flow of the coating. These structures are much too complicated, or too fragile, to be developed by variations in the sputter yield with angle, which is the basis for non-impurity cone theory. The bending of the cones clearly indicates that the structures are plastic, not simply products of sputter erosion. However, these effects are observed at temperatures far below the system melting point.

From thermal considerations,[28] the impact of an energetic ion in this energy range may induce local temperature increases of 1000-3000°C. The lifetime of these thermal enhancements is short, in the range of 10^{-10} seconds. The ion flux in this case to this enhanced area ($\sim 10^4$ $Å^2$) is 10^4 sec^{-1}, which leaves little memory of the previous ion when the next one arrives. In a thin film, particularly on such a localized scale, some thermal enhancement might be expected due to differing thermal properties between the film and the bulk allowing for phonon reflection at the interface as well as from the lateral boundaries of the film.

A contributing factor in the appearance of these liquid-like effects may be the presence of dislocations, particularly those induced by the ion beam. Observations from FIM work, indicate that at ion energies in the range used in this work, damage can be induced to a

depth of 110 Å.[29] From the dislocation theory of melting, viscous flow might be expected in the presence of large numbers of dislocations.[30] This usually occurs at temperatures approaching melting, but in this case may happen at lower values due to the increased dislocation density caused by the ion bombardment. Understanding the quasi-liquid behavior of ion bombarded material may be significant where ion beam sputtering is used for high resolution patterning. It may also be important in developing a more thorough understanding of non-equilibrium processes on surfaces undergoing ion bombardment.

V. ION IMPACT ENHANCED SURFACE DIFFUSION

Low energy ion bombardment of surfaces is used in numerous areas of thin film processing and surface analysis. The basic process of interest is sputtering, which is used for cleaning of surfaces, deposition of films, depth profiling, and etching of various patterns on micron or submicron scales. The ion bombardment also induces diffusion of bulk or impurity atoms on the surface[31-33] or in near-surface regions.[34,35] This induced diffusion is in addition to the normally occurring thermal diffusion and, depending on experimental circumstances, can be the dominant process. Enhanced surface adatom mobility has been reported during ion bombardment of Ag on glass substrates,[31] and of W atoms on W field emission tips.[32,33]

The present experiment utilized the formation of impurity induced sputter cones on Cu and Al substrates during Ar^+ ion bombardment as a measure of the surface adatom diffusion. The formation of these cones is attributed to the enhanced surface diffusion and resulting nucleation of impurity adatoms on the surface.[22] The magnitude of this enhanced diffusion is related to the current density of the incoming ions. The spacing of the resulting diffusion leading to lower areal densities of cones.

The ion source sputtered the sample with Ar^+ at 1000 eV and a current density variable from 0.1 to 2.7 mA/cm^2. The samples were typically 1 cm^2 in size with a temperature set point from 50°C to 600°C. Any sample heating due to increased power flux at high current density was taken into account by reducing the power to the sample heater.

When the incoming ion current density was varied at constant temperature, and the sputtering time adjusted to yield a constant dose,

the dependence of the cone spacing on current density is determined. Figures 8a and 8h are a series of micrographs showing density reduction with current density. Some of the measurements on similar samples are shown in Fig. 9, for the case of Mo adatoms on Cu at 300°C. Here, particularly at the higher current densities, the cone spacing was approximately proportional to the ion current density. The sample temperatures are measured quite easily and any sample heating due to the increased power flux at high current density was taken into account in setting the power to the sample heater. The dependence of cone spacing on current density was determined for other impurity species on Cu (Fig. 10 and Table 2). In addition, a similar effect has been seen on Al substrates.

As the sample temperature increased, the strength of the dependence of the cone spacing on ion current density also increased as shown in Fig. 10 and Table 2. This behavior would be expected because impacts would provide more enhancement to a more thermally active surface. It should be noted that the data at 400°C in Fig. 10 do not follow the expected trend below about 1.3 mA/cm^2 although the slopes of the upper regions of the three curves are ordered as the temperatures.

An additional experimental observation that should be noted is the variation in cone size with current density at constant ion dose shown in Fig. 8. As the current density was varied from 0.1 to 2.7 mA/cm^2 and the time of sputtering adjusted to provide a constant ion dose, the size of the resultant cone also varied. At the lower values of current density, the cones were droplet-shaped (Fig. 8a). This shape has been described earlier, and is characteristic of the quasi-liquid coating often observed on cone surfaces. As the current density was increased,

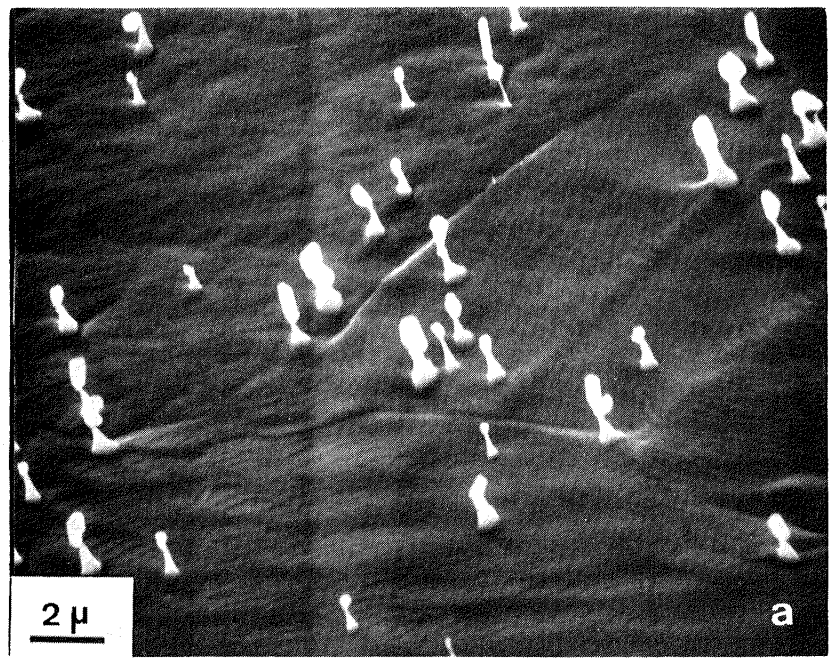

(a) 0.1 mA/cm^2, 500 min.

(b) o.35 mA/cm^2, 142 min.

Fig. 8. Effect of current density at constant ion dose on surface microtexture development. Carbon induced cones on copper. 420°C, 1000 eV Ar^+.

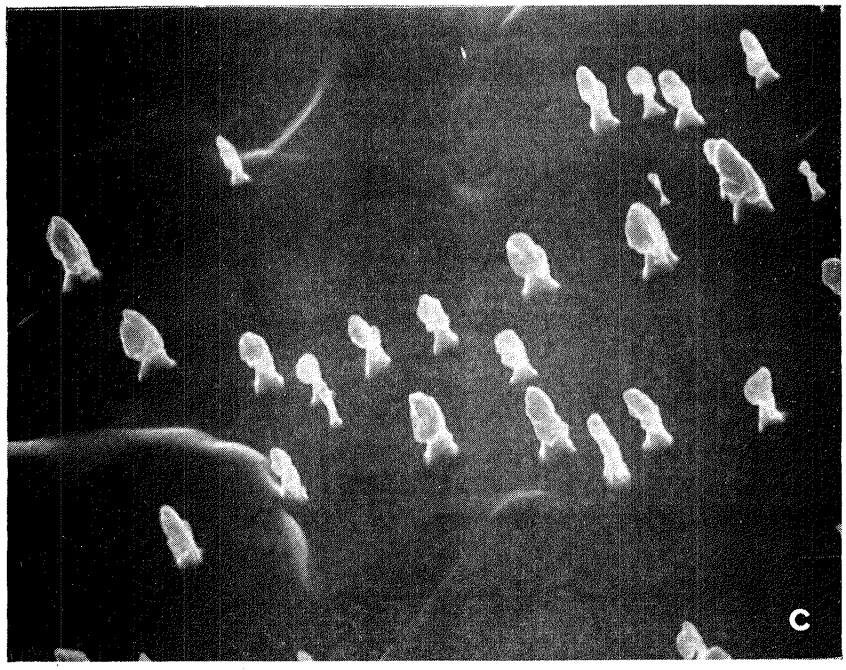

(c) 0.5 mA/cm^2 100 min.

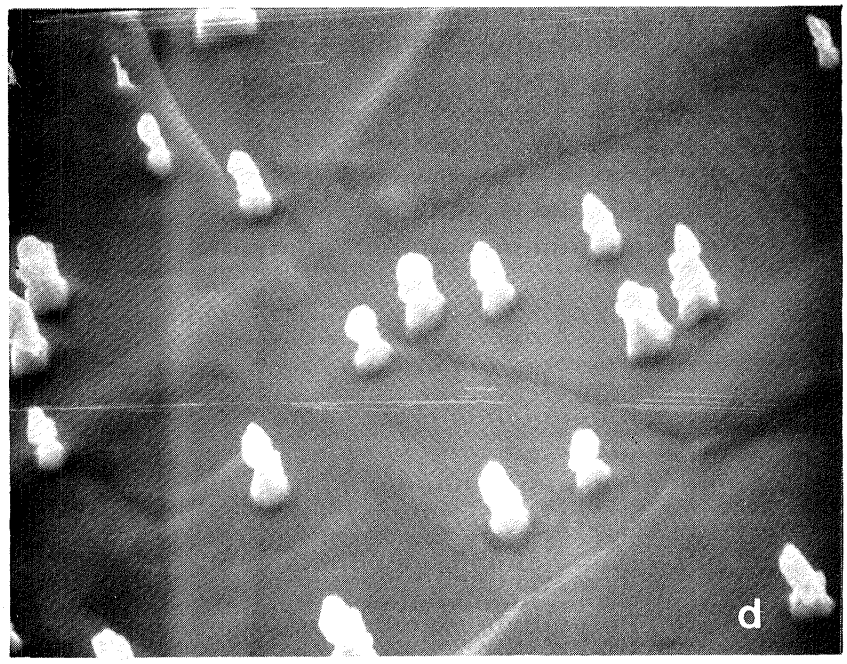

(d) 0.8 mA/cm^2, 62.5 min.

Fig. 8. Continued

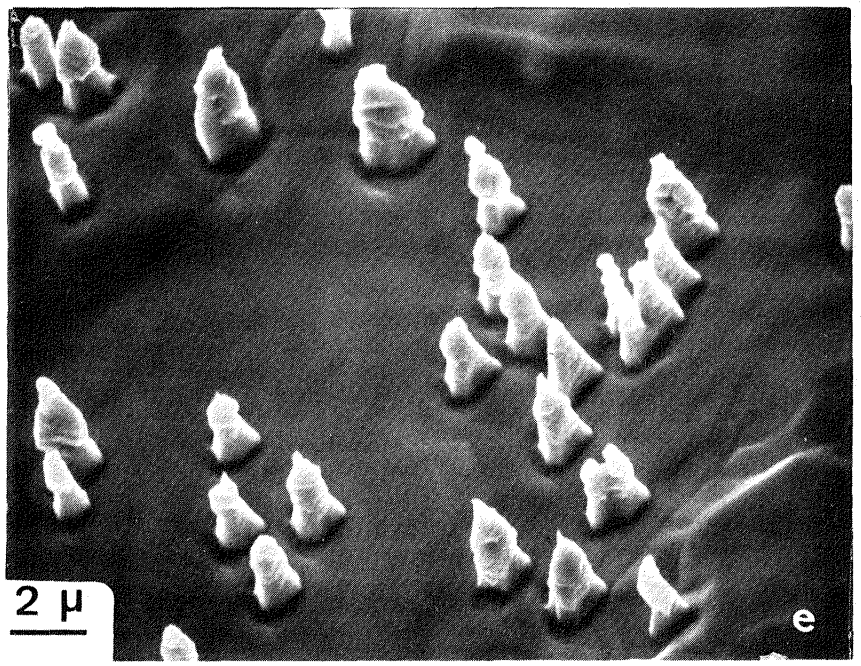

(e) 1.0 mA/cm^2, 50 min.

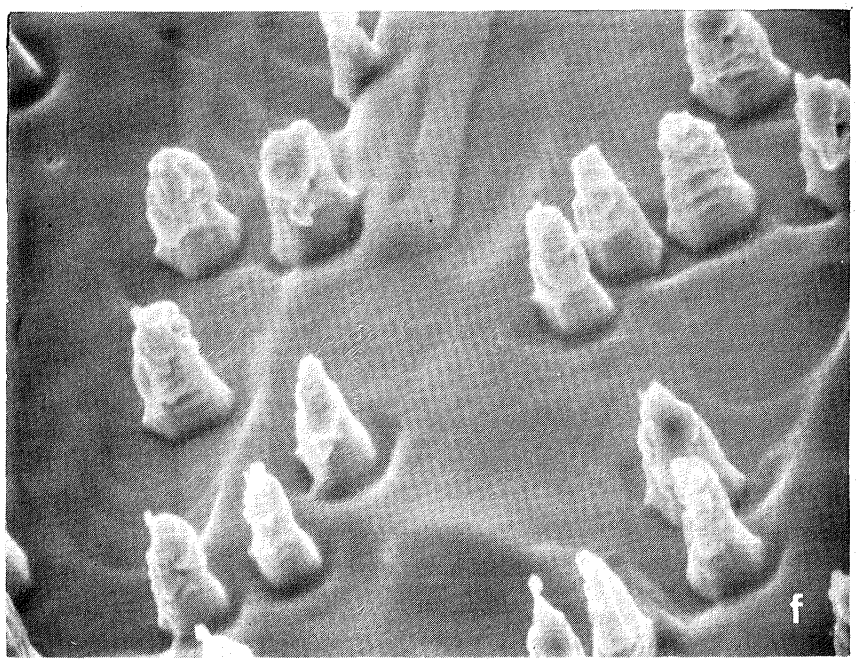

(f) 1.5 mA/cm^2, 33.3 min.

Fig. 8. Continued

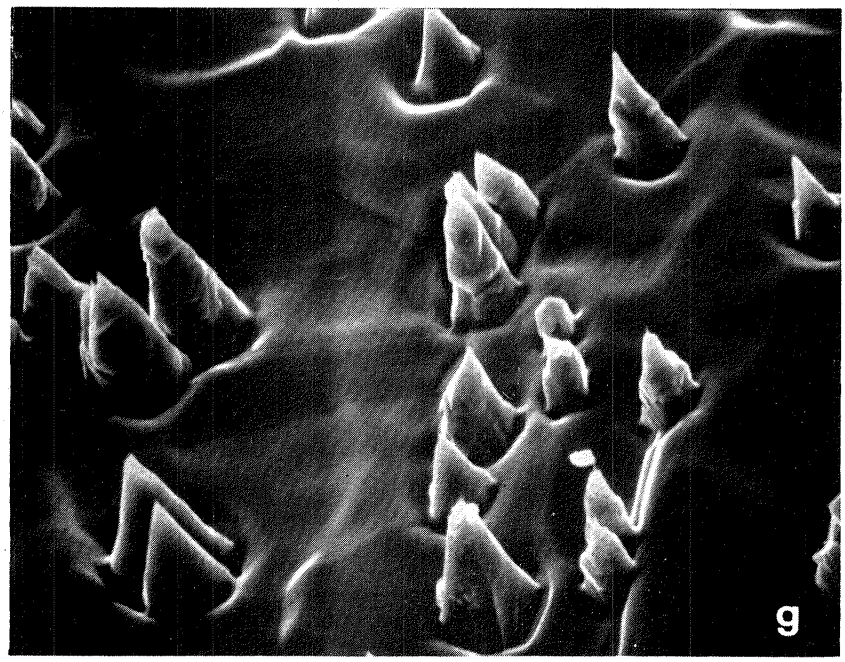

(g) 2.0 mA/cm^2, 25 min.

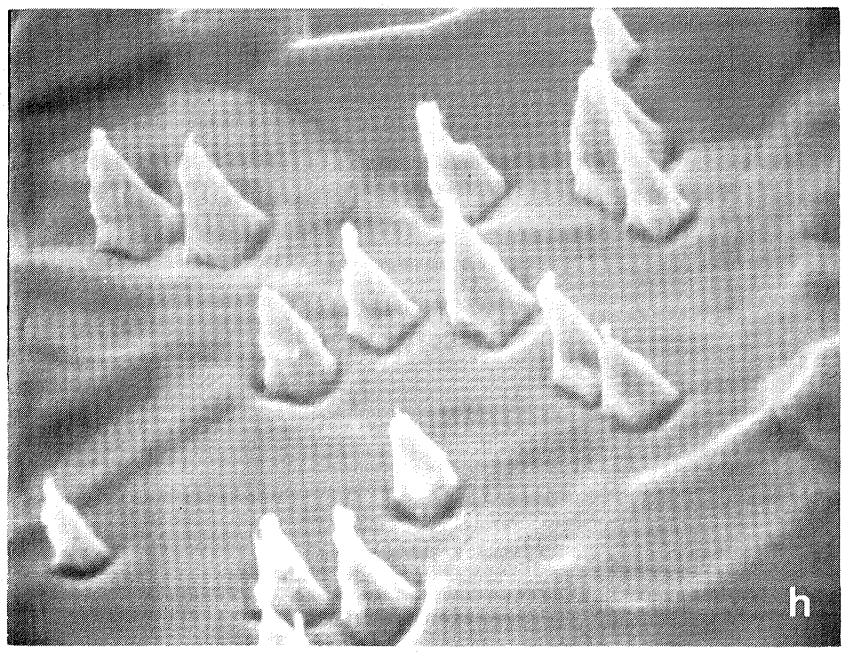

(h) 2.7 mA/cm^2, 18 min.

Fig. 8. Continued

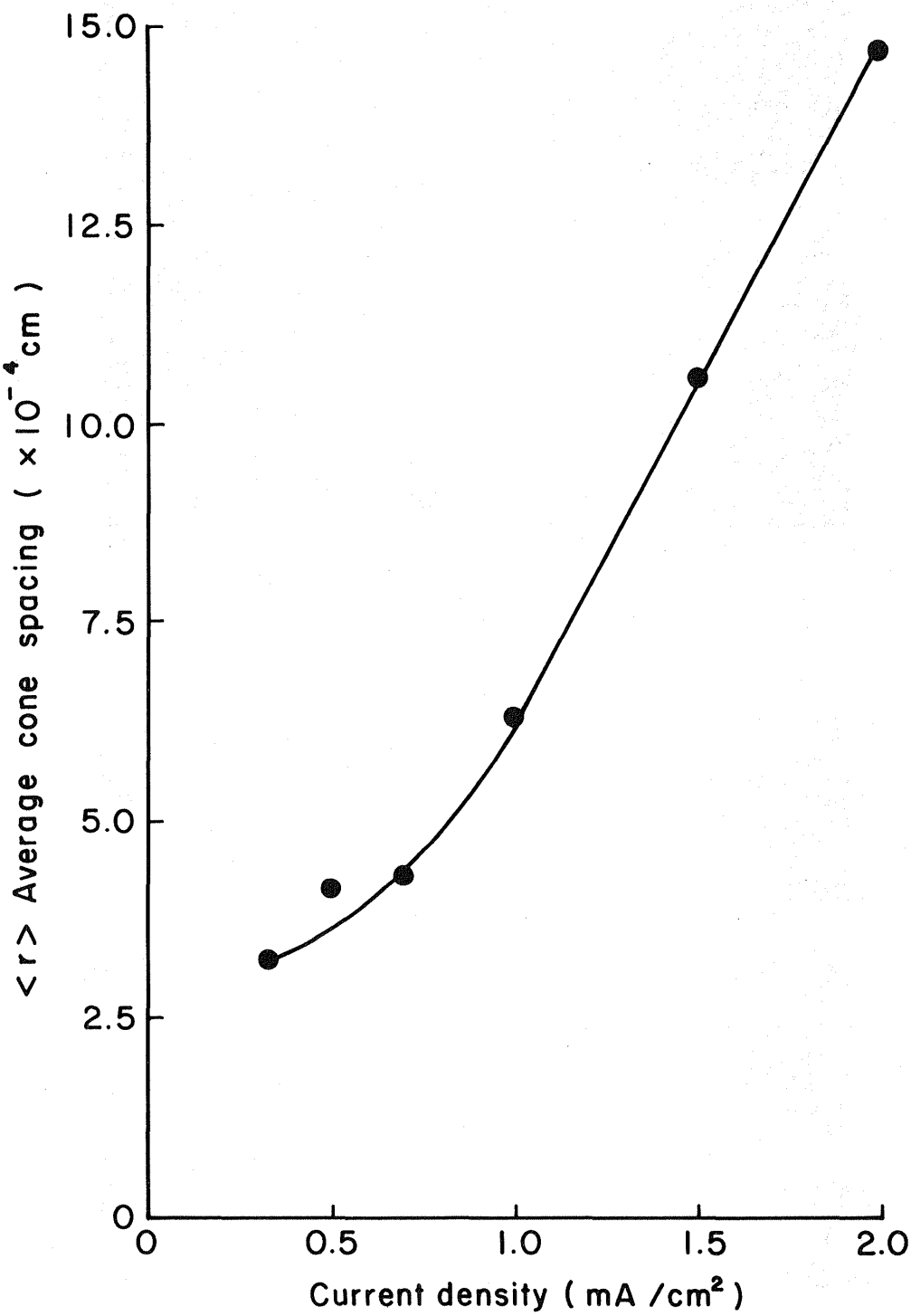

Fig. 9. Average cone spacing as a function of ion beam current density. Sample: Mo induced cones on Cu, 300°C.

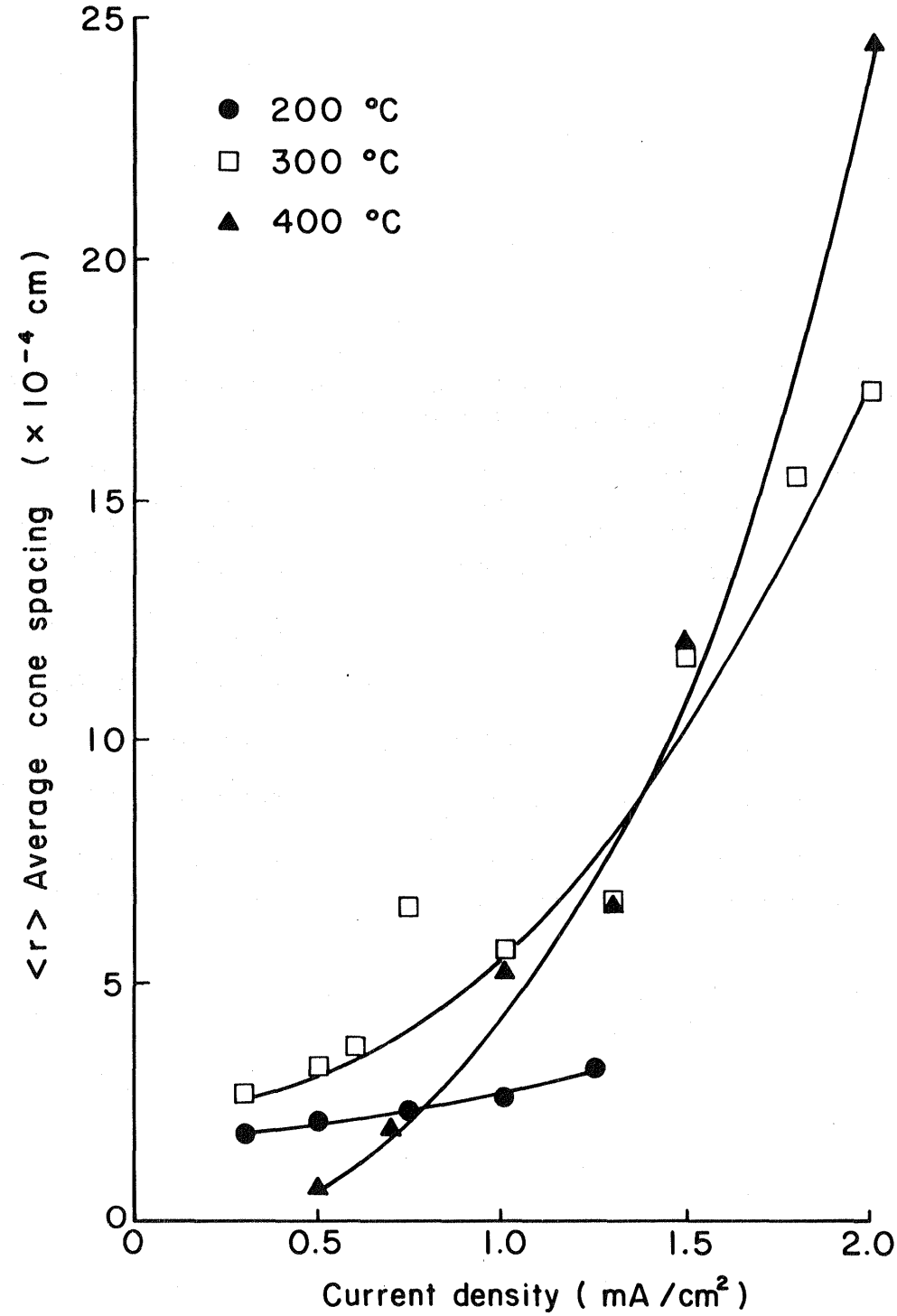

Fig. 10. Average cone spacing as a function of ion beam current density. Sample Ta induced cones on Cu at 200, 300 and 400°C.

Table 2. Slopes at High Current Densities of the Average Cone Spacing Versus Ion Current Density Data.

Sample	Temperature	Slope
C on Cu	400°C	2.1×10^{-4} cm^3/mA
Mo on Cu	300°C	7.2×10^{-4} cm^3/mA
Ta on Aℓ	400°C	2.2×10^{-4} cm^3/mA
Ta on Cu	200°C	1.3×10^{-4} cm^3/mA
Ta on Cu	300°C	8.7×10^{-4} cm^3/mA
Ta on Cu	400°C	1.5×10^{-3} cm^3/mA

the size of cones also increased, and the structure appeared more cone-like, although the protective coating was still evident (Fig. 8e). At the highest current densities, the cones were much larger and the coating is much less evident (Fig. 8h).

Clearly, from the results given in Figs. 9 and 10 and in Table 2, a significantly greater diffusion flux on the surface is being observed than would be expected from thermal diffusion alone. For purely thermal diffusion, impurity adatoms diffuse on the surface of the sample with a characteristic length[22]

$$r = r_o \exp^{-E_d/2kT}$$

where E_d is the activation energy for surface diffusion, and r_o is given as

$$r_o = (E_d/2m)^{1/4} \ (N_o^{1/3}/R\sigma)^{1/2}$$

where m is the adatom mass, σ its sputtering cross section, N_o the bulk atom density, and R the incoming ion current density. These diffusing adatoms can form stable clusters which are then associated with the sputter cones that form with continued sputtering. The spacing between clusters can be identified with twice the characteristic length described above.[22] According to this model, holding the temperature constant and varying the current density should produce an $R^{-1/2}$ dependence in the cone spacing. A much different dependence is observed experimentally (Figs. 9 and 10). The dependence at higher ion current densities is approximately linear.

The interpretation placed on the observed behavior is that ion impacts are enhancing the diffusion of adatoms along the surface by inducing more jumps or steps in the adatom's random walk. The thermal diffusion model did not include this mechanism for motion on the surface.

If the observed diffusion of an adatom on the surface is viewed as the result of a random walk, the average path length is related to the number of single-site jumps or steps N_s by

$$\langle r \rangle = a_o \sqrt{N_s}$$

where a_o is the average spacing between adsorption sites. It should be noted that N_s refers to the number of steps of size a_o that result in a net average translation of $\langle r \rangle$. If a_o were varied, a smaller number of larger steps could yield an equivalent result.

The total number of jumps under consideration is the sum of the ordinary thermally induced diffusion jumps activated at the equilibrium substrate temperature plus any jumps induced by ion impact, thus

$$N_S = N_T + N_I$$

where N_T is the number of thermal jumps and N_I is the number of ion impact induced jumps. Both processes would be summed over the average lifetime τ of an adatom on the surface. The number of thermal diffusion jumps is[22]

$$N_T = \nu_o \exp(-E_d/kT)\tau$$

where ν_o is an attempt frequency. If each incident ion is assumed to generate N_i single-step jumps on the average, under specified conditions, then the total number of ion impact induced jumps experienced by an adatom during its lifetime is given by

$$N_I = N_i R\tau/n$$

where n is the density of adatoms on the surface and R is the ion arrival rate per unit area. The magnitude of n for typical conditions is found both from combination measurement and calculation to be about 0.1 to 2% of a monolayer.[20] The average lifetime for a single diffusing adatom is

$$\tau = 1/R\sigma$$

where σ is a cross section for removal that incorporates the sputter yield of the isolated adatom. N_i will, in general, be some function of the ion current density. From the rough linearity of the average cone spacing with current density at high current densities found in Figs. 9 and 10, the number of induced jumps per ion appears to be proportional to the square of the current density. In the limit of very low current densities, however, such a nonlinear relation would clearly fail. N_i would also logically be dependent on some of the other fundamental parameters such as adatom density, ion energy, substrate type and temperature, and adatom species.

Using the technique outlined, the number of induced jumps per incident ion can be calculated from the experimental data. For the data plotted in Fig. 10, the calculated numbers of induced jumps are given in Table 3.

Table 3. Induced Jumps Per Incident Ion.

R	N_i		
mA/cm^2	200°C	300°C	400°C
0.30	115	199	-
0.50	141	320	18
0.75	169	-	-
1.00	217	1120	928
1.25	320	1470	1470
1.50	-	4160	4470
2.00	-	9600	19200

The number of induced adatom jumps at the lower current densities are of similar magnitude to those found in field emission studies of diffusion.[33] This work was concerned with self-diffusion, however, so the values correspond to the numbers of displaced surface atoms rather than dissimilar diffusing adatoms.

The strong nonlinearity in the dependence on R shown in Table 3 is possibly indicative of cooperative processes in which the surface movement of adatoms from one ion impact depends on the spatial or temporal proximity of other ion impacts.

In the wake of an ion impact on the surface, there will be some resulting time-dependent distribution of the deposited energy in the substrate. For the study of surface diffusion, attention can be focused on a circular area of the surface centered on the impact site. If only the simplest model is considered, the circular area can be viewed on the average as being a zone of thermal enhancement that dissipates abruptly after a characteristic time. This approach is similar to that of Thompson and Nelson in their sputtering work.[36] Such an approach is not satisfactory for detailed calculations but can provide some measures of typical times and temperatures involved in the enhanced diffusion process.

For enhanced surface diffusion, the probability of an adatom jumping to a new site is proportional to $\exp(-E_d/(kT + E_T))$ where E_T represents the local thermal enhancement of the impacting ion or ions. As current densities increase, cooperative effects become more probable in which the effects of one ion impact have not fully dissipated before another impact occurs in the affected area. The overlap of two areas of ion impact thermal enhancement would have a probability proportional to

R^2; thus, for a given temperature, the number of ion impact induced jumps in such regions would be proportional to R^2.

It is often instructive to consider this impact enhanced diffusion as an effective temperature averaged over the surface. This has been done in other studies as a measure of the enhanced surface diffusion either in condensation[31] or in field emission cases,[32,33] or as a measure of the epitaxial temperature in ion assisted vapor deposition.[37,38] The effective temperature is found simply by setting the experimentally determined diffusion coefficient, or in this case the random walk path length, equal to the theoretically determined relation using thermally activated diffusion only and solving for the temperature. This effective temperature will obviously be a function of current density. The results for the case of Mo impurities on Cu at 573°K are shown in Table 4. These temperatures, particularly at the higher current densities where the effective temperature approaches the melting point are not physically achievable values, but merely a means of estimating the magnitude of diffusion under ion bombardment conditions. The fact that the effective temperatures for diffusion can approach the melting temperature gives a rough quantitative agreement with the observation of quasi-liquid behavior.

The experimental data appear to confirm the existence of ion impact enhanced surface diffusion. Although an adequate model has not been developed to include both thermal and impact enhanced diffusion, one is required if data are to be properly interpreted at current densities greater than a few tenths of mA/cm^2.

Table 4. Effective Temperatures for Mo on Cu.

R (mA/cm^2)	T_o	T_{eff}
.3	573°K	580
.5	573	633
1.0	573	798
1.5	573	1012
2.0	573	1241

VI. COMPUTER MODELING OF ION BEAM SPUTTERING IN TWO DIMENSIONS

When surfaces undergo ion bombardment, changes in the surface topography are noted. This has been the subject of numerous experimental and theoretical studies. The most dominant effect in the formation of topography changes during sputtering is the dependence of the sputtering yield on angle of incidence of the ion. This effect is relatively small at angles near perpendicular, but rises smoothly to several times the perpendicular values at angles in the range of 50-70° from perpendicular, then falls to zero at grazing incidence (90°). From this dependence, several models of topography development have been formulated. Stewart and Thompson[39] showed how triangular facets could erode by the motions of intersecting semi-infinite planes. From this early analytic model, Cantana, et al.[40] developed a digital, interval model that broke the surface into individual intervals which were then sputtered separately. This model was not very successful and the interval approach was dropped in most subsequent models. Barber, Frank, et al.[41] developed a model based on Frank's theory of crystal dissolution. This model is graphical and uses an "erosion slowness" curve to follow the development of the surface. Other, similar analytic methods have been applied by Carter, et al.[42] and by Kelly and Auciello.[43] Computer-based analytic models have been developed by Ducommon, et al.[44,45] In the second of these articles, computer-modeled topography was compared to experimental results in the erosion of a step with good agreement.

These models are based only on sputtering and are two-dimensional. Smith and Walls[46] have developed a three-dimensional form of these models, and Lehman, et al.[47] have included redeposition in a computer simulation.

The coning process involves numerous features of ion-surface interaction. Dominant among these probably is the angle dependent sputtering yield described above. But also the processes of ion reflection, redeposition of sputtered material, surface diffusion (thermal and enhanced) and possibly "quasi-liquid" motion of the coating on the cones have to be considered.

Presently, a computer model has been developed to describe the sputtering and reflection process of any arbitrary surface shape. This model is in digital, or interval format, unlike the above-described analytical, and computer-analytic models. This model describes the surface two-dimensionally, as in a cross section of the surface viewed from the side. The surface is then divided into 270 intervals. The intervals are of equal length in the x direction only. This allows use of a simple sputtering rate, without having to multiply in the cosine of the surface inclination angle to take into account the reduced effective current density onto a steep surface. The modeling is as follows: one of the 270 intervals is selected at random, the slope of this interval is determined, the relative sputtering yield is then determined by calculating the angle between the incoming ion and the interval, using the chart of sputter yield vs. angle, and subtracting from the interval the appropriate amount. The total process then repeats at another randomly chosen interval. After 5,000 to 20,000 steps (20-80 per interval), the resulting surface shape is displayed. This is typically not the final result, but an indication of the type of changes the surface is undergoing. Generally 200,000 to 1,000,000 steps are needed to completely "develop" the final topography. The reason for the large number of steps is that, due to the relatively small number of horizontal intervals on the surface, the relative amount subtracted from

each needs to be very small. Otherwise, artificial angles will develop at the subtracted points. Usually some smoothing is also needed for this same reason. The smoothing used presently is a 3-pt average. This ideally smooths the surface on a microscopic scale and does not affect large-scale developments.

Additionally, reflection of the incident ions can be added to this model. Once the angle of the surface with respect to the ion beam is determined, the ion can be allowed to reflect from the surface at that same angle. This ion can then be followed until it intersects with the surface (if it ever does) at some other point. At this other point it has some probability of sputtering. The amount of sputtering is gauged by the reflection coefficient (which is between 0 and 1). The reflection coefficient can be estimated from the literature,[48] although values for configurations of interest are difficult to find. Generally, the reflection coefficient is equal to 0 for angles from 0 to 30-40°. It then increases to 1 at ∿85-90°. A simplified version is used in the present model. The reduced energy function is related to the loss of energy by the ion during the reflection. This will cause the sputtering yield of the reflected ion (atom) to be effectively reduced. The energy reduction function will be close to 1 in the present case (little energy loss) because the sputtering yield is relatively insensitive to energy in this range (500-1000 eV). The effect of energetic sputtered particles[43] will be ignored here, also due to the low energy range for incident ions.

With the present model, any initial shape can be followed as it undergoes sputtering and the associated reflection sputtering. In the past, the analytic models have had to rely on simple, geometrical shapes, often sine waves, to describe the initial surface.[40-45]

These shapes, although not really characteristic of physical surfaces, led to reasonable conclusions about the final topography. Numerous shapes have been chosen and simulated, from simple lines (flat planes) to very rugged, rapidly varying shapes. Only the relatively simple shapes are shown here. Figure 11a shows the development in time of a simple ridge. The top line is the initial unsputtered surface. The ion flux is incident from the top of the figure and the bulk material is below the line. Successive iterations or intervals in sputtering time lead to the successively lower contours. The array of lines follows the surface with time. Figure 11 was generated in the absence of reflection and shows simply the effect of primary sputtering. The two main factors are: (a) the ledge quickly becomes a wall of angle equal to the maximum yield of the sputter yield vs. incident angle relation. This wall "moves" with time into itself, and (b) the plane below the wall does not completely flatten out after the wall has "moved away" but retains a gradual slope for a long period of time. Figure 11b shows two closely located edges which, in cross-section, at times looks somewhat cone-like in appearance. Figure 12 shows the contribution of reflection to the problem. Starting with a cone-like shape, the successive sputter-iterations are seen in Fig. 12a without any reflection. In Fig. 12b, reflection is included with a unit reduced energy function (i.e., = 1.0). This is the maximum allowed effect for reflection in this case. Values for the reduced energy function of less than 1 lead to intermediate behavior, although below 0.90, the structures apparently always erode away with time. It is not clear at present whether the topography of Fig. 12b will eventually erode.

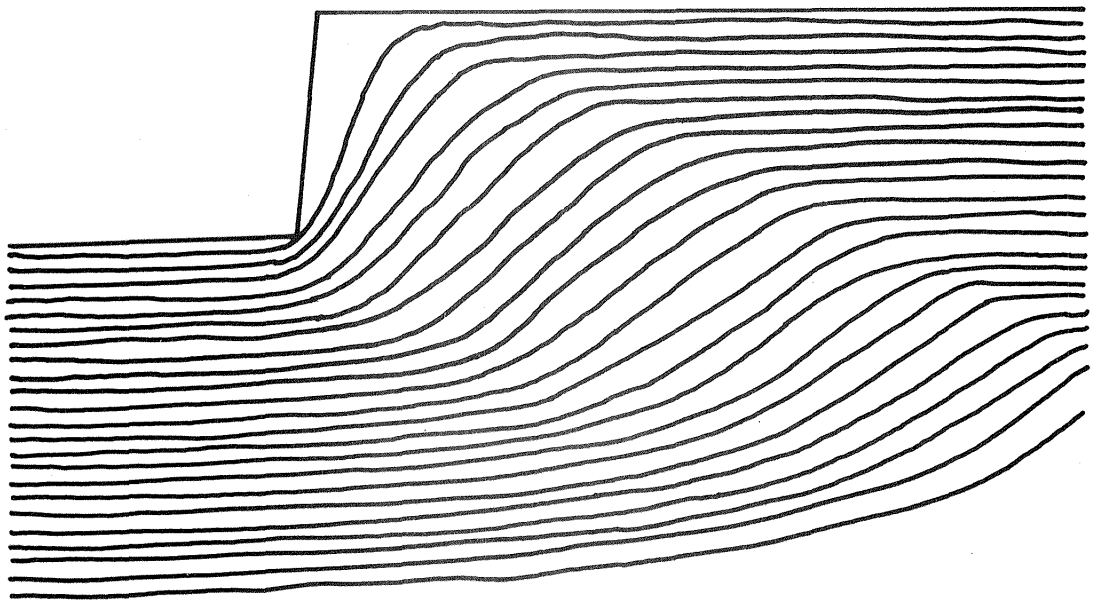

(a) Single edge.

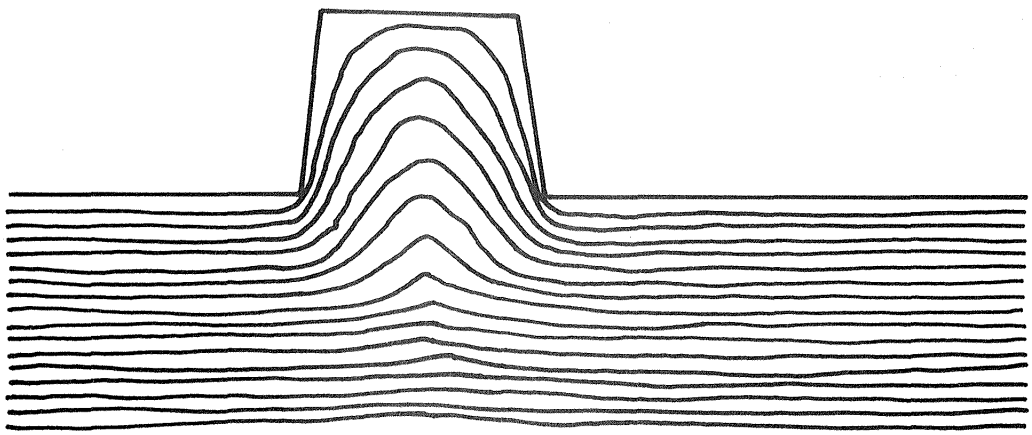

(b) Double edge.

Fig. 11. Calculated time development of sputtered surfaces without ion reflection.

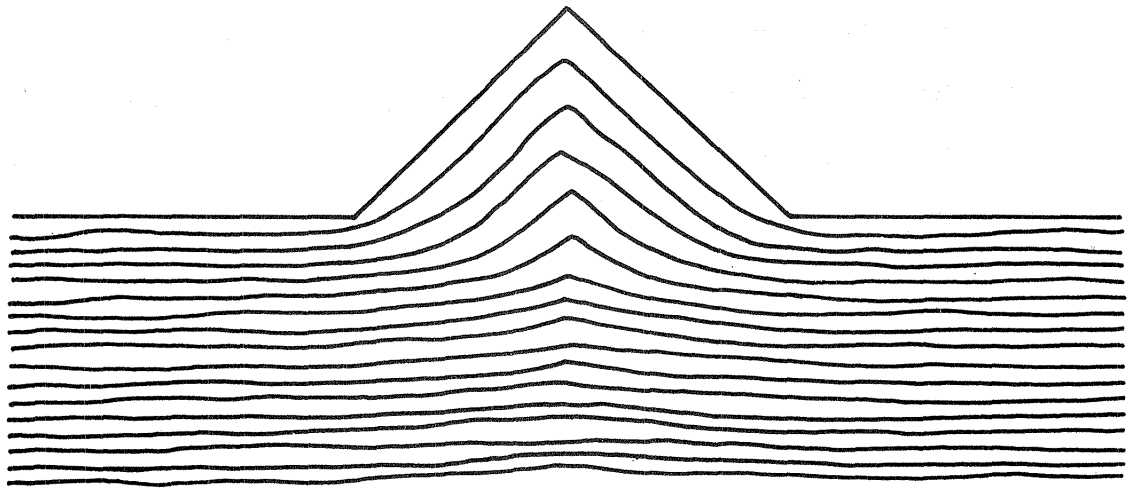

(a) Without ion reflection.

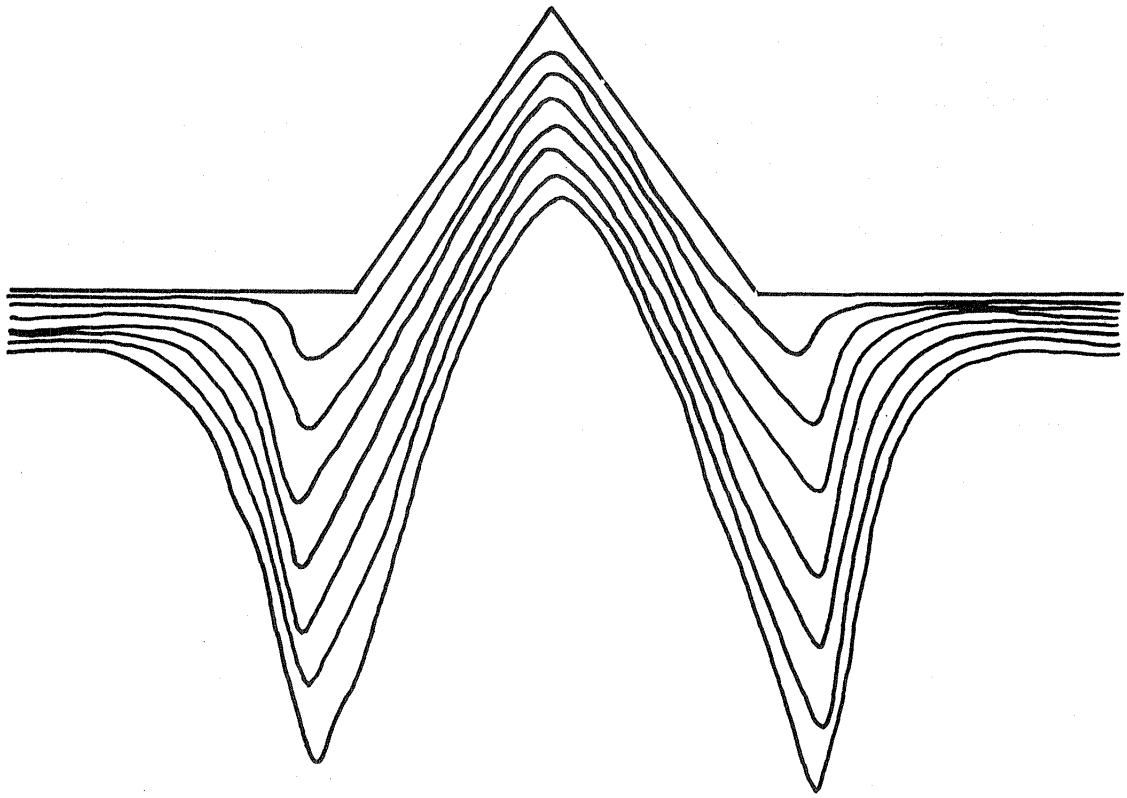

(b) Including ion reflection.

Fig. 12. Calculated time development of a sputtered cone-like shape with and without ion reflection.

Numerous other shapes have been modeled with this program: pits, square wave shapes, planes, spikes, convoluted, rugged shapes, and others. The general results are as follows: without reflection the final shape for almost all initial topography is a flat plane. The partial exceptions to this are an infinite ridge, which will form a wall of angle θ equal to the maximum sputter yield angle which moves with time, and a sharp feature, which will produce an area of angle approaching 0 (flat plant), but will take a very long time to actually do this. This is due to the small slope of the sputter yield versus angle curve as the angle approaches zero.

With reflection, the final topography shapes are similar to the case without reflection if the reduced energy function is <0.90. Above 0.90, it is possible that non-planar topography may be semi-stable, or may even enlarge with time. This latter case is evident in numerous experimental studies of non-impurity coning. Here, initial small asperities or bumps form into cones much larger than the original asperity or bump. Without reflection this is not possible. Any shape would become smaller not larger. With reflection, enlargement is possible, although it may only be temporary.

VII. CONCLUDING REMARKS

The main areas of study during the final phase of this work include: optical properties of microtextured surfaces, quasi-liquid behavior of surface material under ion bombardment, ion impact enhanced surface diffusion and computer simulation of the development of surface topography under ion beam sputtering.

Ion beam microtextured optical absorbers have been generated and tested. Because the texture has dimensions of the order of the wavelength of visible light, these surfaces can be highly absorbing. Of the structures studied, the wave-like formations seem to be the most efficient absorbers.

Optical absorptance has been measured for a number of textured surfaces. Absorptances from 0.90-0.97 have been measured for the wavelength range 0.4-2.2 μ. Total emissivities measured by vacuum cooling were in the range of 0.2-0.3. Liquid-like properties have been observed on surface structures developed by means of ion beam microtexturing. The structures include cones, pyramids, or wave-like formations. The observed liquid-like effects are droplet formation, the apparent flow and coalescence of closely packed structures, wetting angle and other surface tension effects, and the bending of cones by additional heating. The substrate temperatures are in the range of 50-600°C and therefore cannot explain the presence of the "quasi-liquid" effects. These effects are also seen to some extent on Cu, Al, Au, Pb, and Ni substrates.

Ion impact enhanced surface diffusion has been observed in several systems undergoing Ar^+ ion bombardment over a current density range from

.3 to 2.7 mA/cm^2. The magnitude of this effect is often greater than the magnitude of the normally occurring thermal surface diffusion, and the effect can be described in terms of an effective surface temperature and possible cooperative effects of multiple ion impacts in a localized region. In addition, differences have been observed in the size of sputtered structures as a function of current density at constant dose.

A computer program has been written to model the development of sputtered topography. This two-dimensional model basically follows the pattern of earlier programs except that ion reflection has been incorporated. This more realistic simulation yields developing structures that bear a striking resemblance to the cross section of a sputter cone surrounded by a trough.

REFERENCES

1. R. S. Berg and G. K. Kominiak, "Surface Texture by Sputter Etching," J. Vac. Sci. Technol., Vol. 13, No. 1, pp. 403-405 (Jan./Feb. 1977).

2. R. S. Robinson and C. M. Haynes, "Surface Texturing," Industrial Ion Source Technology, NASA CR-135353, pp. 24-75 (Nov. 1977).

3. G. K. Wehner and D. J. Hajicek, "Cone Formation on Metal Targets during Sputtering," J. Appl. Phys., 42, pp. 1145-1149 (Mar. 1971).

4. J. J. Cuomo, J. F. Ziegler, and J. M. Woodall, "A New Concept for Solar Energy Thermal Conversion," Appl. Phys. Lett., Vol. 26, No. 10, pp. 557-559 (May 1975).

5. B. A. Banks, A. J. Weigand, C. A. Babbush, and C. L. Van Kampen, "Potential Biomedical Applications of Ion Beam Technology," AIAA Paper No. 76-1018, AIAA International Electric Propulsion Conference, Key Biscayne, Florida (Nov. 14-17, 1976).

6. W. R. Hudson, "Nonpropulsive Applications of Ion Beams," AIAA Paper No. 76-1015, AIAA International Electric Propulsion Conference, Key Biscayne, Florida (Nov. 14-17, 1976).

7. A. J. Weigand and B. A. Banks, "Ion-Beam-Sputter Modification of the Surface Morphology of Biological Implants," J. Vac. Sci. Technol., Vol. 14, No. 1, pp. 326-331 (Jan./Feb. 1977).

8. W. R. Hudson, "Ion Beam Texturing," J. Vac. Sci. Technol., Vol. 14, No. 1, pp. 286-289 (Jan./Feb. 1977).

9. P. K. Agarwal, E. L. Park and A. J. Weigand, "Ion Beam Texturing of Heat Transfer Surfaces," AIAA Paper No. 81-0670, AIAA/JSASS/DGLR 15th International Electric Propulsion Conference, Las Vegas, Nevada (April 21-23, 1981).

10. C. A. Spindt, "Physical Properties of Thin Film Field Emission Cathodes with Molybdenum Cones," J. Appl. Phys., 46, p. 5248 (1976).

11. R. Forman, "Secondary Electron Emission Properties of Conducting Surfaces with Application to Multistage Depressed Collectors for Microwave Amplifiers," NASA Technical Paper 1097 (1977).

12. J. J. Cuomo, U.S. Patent No. 4,005,698.

13. D. P. Grimmer, K. C. Herr, and W. J. McCreary, "Possible Selective Solar Photothermal Absorber: Ni Dendrites Formed on Al Surfaces by the CVD of Ni $(CO)_4$," J. Vac. Sci. Technol., Vol. 15, No. 1, pp. 59-64 (Jan./Feb. 1978).

14. J. J. Cuomo, J. M. Woodall, and T. H. DiStefano, "Dendritic Tungsten for Solar Thermal Conversion," Proceedings of the American Electroplaters' Society Coatings for Solar Collectors Symposium, Atlanta, GA, p. 133 (1976).

15. C. R. Baraona and H. W. Brandhorst, "V-Grooved Silicon Solar Cells," Conference Record of the 11th Photovoltaic Specialists Conference, Phoenix, AZ, p. 44 (May 1975).

16. H. G. Craighead, R. E. Howard, J. E. Sweeney, and D. M. Tennant, "Textured Surfaces: Optical Storage and Other Applications," J. Vac. Sci. Technol., Vol. 20, p. 316 (1982).

17. S. M. Rossnagel and R. S. Robinson, "Summary Abstract: Optical Properties of Ion Beam Microtextured Surfaces," J. Vac. Sci. Technol., Vol. 20, p. 336 (1982).

18. P. M. Curmi and G. L. Harding, "Surface Texturing of Copper by Sputter Etching with Applications for Solar Selective Absorbing Surfaces," J. Vac. Sci. Technol., Vol. 17, p. 1320 (1980).

19. R. S. Robinson, "Ion Beam Microtexturing of Surfaces," NASA CR-165383, May 1981.

20. S. M. Rossnagel and R. S. Robinson, "The Time Development of Impurity Generated Sputter Cones on Copper," Radiation Effects Letters, Vol. 58, pp. 11-16 (1981).

21. S. M. Rossnagel and R. S. Robinson, "Surface Diffusion Activation Energy, Determination using Ion Beam Microtexturing," J. Vac. Sci. Technol., Vol. 20, No. 2, pp. 195-198 (Feb. 1982).

22. H. R. Kaufman and R. S. Robinson, "Ion Beam Texturing of Surfaces," J. Vac. Sci. Technol., Vol. 16, No. 2, pp. 175-178 (Mar./Apr. 1979).

23. R. S. Robinson, "Physical Processes in Directed Ion Beam Sputtering," NASA CR-159567 (March 1979).

24. R. S. Gvosdover, V. M. Efremenkova, L. B. Shelyakin and V. E. Yurasova, "Formation of Cones during Sputtering," Rad. Eff. Vol. 27, p. 237 (1976).

25. R. S. Williams, R. J. Nelson and A. R. Schlier, "Depth Resolution Degradation of Sputter-Profiled InP/$In_sGa_{1-x}As_yP_{1-y}$ Interfaces Caused by Cone Formation," Appl. Phys. Lett., Vol. 36, p. 827 (1980).

26. W. R. Hudson, A. J. Weigand, and M. J. Mirtich, "Optical Properties of Ion Beam Textured Metals," NASA TM X-73598, (1977).

27. S. M. Rossnagel and R. S. Robinson, "Quasi-Liquid States Observed on Ion Beam Microtextured Surfaces," J. Vac. Sci. Technol., Vol. 20, p. 506 (1982).

28. R. Kelley, "Theory of Thermal Sputtering," Rad. Eff., Vol. 32, p. 91 (1977).

29. R. D. Webber and J. M. Walls, "The Structure and Topographical Modification of Surfaces During Depth Profiling," Thin Solid Films, Vol. 57, p. 201 (1979).

30. J. G. Dash, Films on Solid Surfaces, Academic Press, NY (1975).

31. M. Marinov, "Effect of Ion Bombardment on the Initial Stage of Thin Film Growth," Thin Solid Films, Vol. 46, p. 267 (1977).

32. Zh. I. Dranova and I. M. Mikhailovskii, "Low Temperature Surface Migration of Tungsten, Activated by Ion Bombardment," Soviet Physics-Solid State, Vol. 12, p. 104 (1970).

33. J. Y. Cavaille and M. Drechsler, "Surface Self Diffusion by Ion Impact," Surf. Sci., Vol. 75, p. 342 (1978).

34. L. Rivaud, I. H. Ward, A. H. E. Houkhy, and J. E. Greene, "Enhanced Diffusion and Precipitation in Cu:In Alloys Due to Low Energy Ion Bombardment," Surf. Sci., Vol. 102, p. 610 (1981).

35. A. H. Eltoukhy and J. E. Greene, "Diffusion Enhancement Due to Low-Energy Ion Bombardment During Sputter Etching and Deposition," J. Appl. Phys., Vol. 51, p. 4444 (1980).

36. M. W. Thompson and R. S. Nelson, "Evidence for Heated Spikes in Bombarded Gold from the Energy Spectrum of Atoms Ejected by 43 keV Ar^+ and Xe^+ Ions," Phil. Mag., Vol. 1, p. 2015 (1962).

37. S. Shimizu and S. Komiya, "The Effects of Low Energy Ions in Silicon Molecular Beam Deposition," Proceedings of the Fifth Symposium on Ion Sources and Ion Assisted Technology, Kyoto, Japan, 435, (June 1981).

38. V. O. Babaev, Ju V. Bykov, and M. B. Guseva, "Effect of Ion Irradiation on the Formation, Structure and Properties of Thin Metal Films," Thin Solid Films, Vol. 38, p. 1 (1976).

39. A. D. G. Stewart and M. W. Thompson, "Microtopography of Surfaces Eroded by Ion-Bombardment," J. Mat. Sci., Vol. 4, p. 56 (1969).

40. C. Cantana, J. S. Colligon, and G. Carter, "The Equilibrium Topography of Sputtered Amorphous Solids, III, Computer Simulation," J. Mat. Sci., Vol. 7, p. 467 (1972).

41. D. J. Barber, F. C. Frank, M. Moss, J. W. Steeds, and I. S. T. Tsony, "Prediction of Ion-Bombarded Surface Topographies using Frank's Kinematic Theory of Crystal Dissolution," J. Mat. Sci., Vol. 8, p. 1030 (1973).

42. G. Carter, J. S. Colligon, and M. J. Nobes, "Analytical Modelling of Sputter Induced Surface Morphology," Rad. Eff., Vol. 31, p. 65 (1980).

43. R. Kelly and O. Auciello, "On the Origin of Pyramids and Cones on Ion Bombarded Copper Surfaces," Surf. Sci., Vol. 100, p. 135 (1980).

44. J. P. Ducommun, M. Cantagrel and M. Marchel, "Development of a General Surface Contour by Ion Erosion," J. Mat. Sci., Vol. 9, p. 72 (1974).

45. J. P. Ducommun, M. Cantagrel and M. Moulin, "Evolution of a Well-Defined Surface Contour Submitted to Ion Bombardment: Computer Simulation and Experimental Investigation," J. Mat. Sci., Vol. 10, p. 52 (1975).

46. R. Smith and J. M. Walls, "The Development of a General Three-Dimensional Surface Under Ion Bombardment," Phil. Mag., Vol. A42, p. 235 (1980).

47. H. W. Lehman, L. Krausbauer and R. Widmer, "Redeposition a Serious Problem in R.F. Sputter Etching of Structures with Micrometer Dimensions," J. Vac. Sci. and Technol., Vol. 14, p. 281 (1977).

48. M. Hou and M. T. Robinson, "The Conditions for Total Reflection of Low Energy Atoms from Crystal Surfaces," Appl. Phys., Vol. 17, p. 371 (1978).

DISTRIBUTION

	Copies
National Aeronautics and Space Administration Washington, DC 20546	
Attn: RS/Mr. Dell Williams, III	1
RTS-6/Mr. Wayne Hudson	1
RTS-6/Mr. Jerome Mullin	1
MT/Mr. Ivan Bekey	1
National Aeronautics and Space Administration Lewis Research Center 21000 Brookpark Road Cleveland, OH 44135	
Attn: Research Support Procurement Section	
Mr. G. Golinski, MS 500-306	1
Technology Utilization Office, MS 3-19	1
Report Control Office, MS 5-5	1
Library, MS 60-3	2
Mr. N. Musial, MS 500-113	1
Dr. M. Goldstein, Chief Scientist, MS 5-3	1
Mr. T. Cochran, MS 501-8	1
Mr. D. Petrash, MS 501-5	1
Mr. N. Grier, MS 501-7	1
Mr. M. Mirtich, MS 501-7	1
Mr. R. Finke, MS 77-4	1
Mr. B. Banks, MS 501-7	1
Mr. D. Byers, MS 501-7	1
Mr. W. Kerslake, MS 501-7	1
Mr. V. Rawlin, MS 501-7	1
Mr. M. Mantenieks, MS 501-7	30
National Aeronautics and Space Administration Marshall Space Flight Center Huntsville, AL 35812	
Attn: Mr. Jerry P. Hethcoate	1
Mr. John Harlow	1
Mr. John Brophy	1
Mr. Robert T. Bechtel	1
Mr. M. Ralph Carruth, Jr.	1
NASA Scientific and Technical Information Facility P.O. Box 8757 Baltimore, MD 21240	
Attn: Accessioning Department	1
National Aeronautics and Space Administration Goddard Space Flight Center Greenbelt, MD 20771	
Attn: Mr. W. Isley, Code 734	1
Dr. David H. Suddeth	1

National Aeronautics and Space Administration
Ames Research Center
Moffett Field, CA 94035
Attn: Technical Library 1

National Aeronautics and Space Administration
Langley Research Center
Langley Field Station
Hampton, VA 23365
Attn: Technical Library 1
Mr. B. Z. Henry 1

The Aerospace Corporation
P.O. Box 95085
Los Angeles, CA 90045
Attn: Dr. B. A. Haatunion 1
Mr. A. H. Silva 1

The Aerospace Corporation
Space Sciences Laboratory
P.O. Box 92957
Los Angeles, CA 90009
Attn: Dr. Y. T. Chiu 1

Bell Laboratories
600 Mountain Avenue
Murray Hill, NJ 07974
Attn: Dr. Edward G. Spencer 1
Dr. Paul H. Schmidt 1

Boeing Aerospace Company
P.O. Box 3999
Seattle, WA 98124
Attn: Mr. Donald Grim, MS 8K31 1
Mr. Russell Dod 1

Case Western Reserve University
10900 Euclid Avenue
Cleveland, OH 44106
Attn: Dr. Eli Reshotko 1

C.E.N.-F.A.R.
Service Du Confinement Des Plasmas
BP6
92260 Fontenay-Aux-Roses,
FRANCE
Attn: J. F. Bonnal 1

Circuits Processing Apparatus, Inc.
725 Kifer Road
Sunnyvale, CA 94086
Attn: Spencer R. Wilder 1

Commonwealth Scientific Corporation
500 Pendleton Street
Alexandria, VA 22314
Attn: George R. Thompson 1

Computing Center of the USSR Academy of Sciences
Vavilova 40
117333 Moscow, B-333
USSR
Attn: Dr. V. V. Zhurin 1

Comsat Corporation
950 L'Enfant Plaza, S.W.
Washington, DC 20024
Attn: Mr. Sidney O. Metzger 1

COMSAT Laboratories
P.O. Box 115
Clarksburg, MD 20734
Attn: Mr. B. Free 1
Mr. O. Revesz 1

CVC Products
525 Lee Road
P.O. Box 1886
Rochester, NY 14603
Attn: Mr. Georg F. Garfield, Jr. 1

DFVLR - Institut fur Plasmadynamik
Technische Universitat Stuttgart
7 Stuttgart-Vaihingen
Allmandstr 124
WEST GERMANY
Attn: Dr. G. Krulle 1

DFVLR - Institut fur Plasmadynamik
33 Braunschweig
Bienroder Weg 53
WEST GERMANY
Attn: Mr. H. Bessling 1

EG & G Idaho
P.O. Box 1625
Idaho Falls, ID 83401
Attn: Dr. G. R. Longhurst, TSA-104 1

Electro-Optical Systems, Inc.
300 North Halstead
Pasadena, CA 91107
Attn: Dr. R. Worlock 1
Mr. E. James 1
Mr. W. Ramsey 1

Electrotechnical Laboratory
1-1-4, Umezono, Sakura-Mura,
Niihari-Gun
Ibaraki,
JAPAN
Attn: Dr. Katsuya Nakayama 1

Fairchild Republic Company
Farmingdale, NY 11735
Attn: Dr. Domenic J. Palumbo 1

Ford Aerospace Corporation
3939 Fabian Way
Palo Alto, CA 94303
Attn: Mr. Robert C. Kelsa 1

General Dynamics
Kearney Mesa Plant
P.O. Box 1128
San Diego, CA 92112
Attn: Dr. Ketchum 1

Giessen University
1st Institute of Physics
Giessen,
WEST GERMANY
Attn: Professor H. W. Loeb 1

Hughes Aircraft Company
Space and Communication Group
P.O. Box 92919
Los Angeles, CA 90009
Attn: Dr. B. G. Herron 1

Hughes Research Laboratories
3011 Malibu Canyon Road
Malibu, CA 90265
Attn: Mr. J. H. Molitor 1
Dr. R. L. Poeschel 1
Dr. Jay Hyman 1
Mr. R. Vahrenkamp 1
Dr. J. R. Beattie 1
Dr. W. S. Williamson 1

IBM Corporation
Thomas J. Watson Research Center
P.O. Box 218
Yorktown Heights, NY 10598
Attn: Dr. Jerome J. Cuomo 1
Dr. James M. E. Harper 1

IBM East Fishkill
D/42K, Bldg. 300-40F
Hopewell Junction, NY 12533
Attn: Mr. James Winnard 1

Ion Beam Equipment, Inc.
P.O. Box O
Norwood, NJ 07648
Attn: Dr. W. Laznovsky 1

Jet Propulsion Laboratory
4800 Oak Grove Drive
Pasadena, CA 91109
Attn: Dr. Kenneth Atkins 1
Technical Library 1
Mr. Eugene Pawlik 1
Mr. James Graf 1
Mr. Dennis Fitzgerald 1
Dr. Graeme Aston 1

Joint Institute for Laboratory Astrophysics
University of Colorado
Boulder, CO 80302
Attn: Dr. Gordon H. Dunn 1

Kyoto University
The Takagi Research Laboratory
Department of Electronics
Yoshidahonmachi Sakyo-ku
Kyoto 606,
JAPAN
Attn: Dr. Toshinori Takagi 1

Lawrence Livermore Laboratory
Mail Code L-437
P.O. Box 808
Livermore, CA 94550
Attn: Dr. Paul Drake 1

Lockheed Missiles and Space Company
Sunnyvale, CA 94088
Attn: Dr. William L. Owens
Propulsion Systems, Dept. 62-13 1
Mr. Carl Rudey 1

Massachusetts Institute of Technology
Room 13-3061
77 Massachusetts Avenue
Cambridge, MA 02139
Attn: Henry I. Smith 1

University of New Mexico
Department of Electrical Engineering
Albuquerque, NM 87131
Attn: Dr. Robert McNeil 1

Optic Electronics Corporation
11477 Pagemill Road
Dallas, TX 75243
Attn: Bill Hermann, Jr. 1

Physicon Corporation
221 Mt. Auburn Street
Cambridge, MA 02138
Attn: H. von Zweck 1

Princeton University
Princeton, NJ 08540
Attn: Mr. W. F. Von Jaskowsky 1
Dean R. G. Jahn 1
Dr. K. E. Clark 1

Research and Technology Division
Wright-Patterson AFB, OH 45433
Attn: (ADTN) Mr. Everett Bailey 1

Rocket Propulsion Laboratory
Edwards AFB, CA 93523
Attn: LKDA/Mr. Tom Waddell 1
LKDH/Dr. Robert Vondra 1

Royal Aircraft Establishment
Space Department
Farnborough, Hants
ENGLAND
Attn: Dr. D. G. Fearn 1

Sandia Laboratories
Mail Code 5743
Albuquerque, NM 87115
Attn: Mr. Ralph R. Peters 1

Tektronix, 50-324
P.O. Box 500
Beaverton, OR 97077
Attn: Curtis M. Haynes 1

Texas Instruments, Inc.
MS/34
P.O. 225012
Dallas, TX 75265
Attn: Larry Rehn 1

TRW Inc.
TRW Systems
One Space Park
Redondo Beach, CA 90278
Attn: Dr. M. Huberman 1
Mr. Sid Zafran 1

United Kingdom Atomic Energy Authority
Culham Laboratory
Abingdon, Berkshire
ENGLAND
Attn: Dr. P. J. Harbour 1
Dr. M. F. A. Harrison 1
Dr. T. S. Green 1

University of Tokyo
Department of Aeronautics
Faculty of Engineering
7-3-1, Hongo, Bunkyo-ku
Tokyo,
JAPAN
Attn: Prof. Itsuro Kimura 1

Veeco Instruments, Inc.
Terminal Drive
Plainview, NY 11803
Attn: Norman Williams 1

University of Iowa
Department of Physics
Iowa City, IA 52242
Attn: Dr. R. T. Carpenter 1

End of Document